Impact Assessment Report

Customer: ESA
Ref. ITT: EOP-SDR/SWO/084-17/DFP
Version: v1.1

Ref. Internal: ARG-003-053_v1r0
Date: 17/06/2021
Filename: Arctic+Salinity_WP500_IAR_v1.1.docx

Signatures

	Name	Signature	Date
Author	Laurent Bertino, NERSC		17-06-2021
Author	Roshin Raj, NERSC		
Author	Jiping Xie, NERSC		
Author	Marta Umbert, BEC		17-06-2021
Author	Carolina Gabarro, BEC		
Approved by	Justino Martinez		
	Carolina Gabarro		17-06-2021
	Rafael Catany		17-06-2021
Authorized by			
Authorized by			

Amendment Record Sheet

	Document Change Record	
Date / Issue	Description	Section / Page
v1.0 (this document)	release to ESA	NA
17/06/2021 / v1.1	Implement feedback from ESA	NA

Table of Content

List of figures

List of tables

Acronyms

AD	Applicable document
ADB	Actions database
ADS	Analysis Dataset
AMOC	Atlantic Meridional Overturning Circulation
ATBD	Algorithm theoretical basis documents
BEC	Barcelona Expert Center
CCD	Closure Contract Documentation
CCI	ESA Climate Change Initiative
CDOM	Colored Dissolved Organic Matter
CDR	Climate Data Record
CMEMS	Copernicus Marine Environment Monitoring Service
CliC	Climate and Cryosphere
CSIC	Consejo Superior de Investigaciones Científicas
DIR	Directory
DNB	Debiased Non-Bayesian
DS	Dataset availability
DUM	Dataset user manual
DVP	Development and validation plan
EC	European Commission
ECMWF	European Centre for Medium-Range Weather Forecasts
EDS	Experimental dataset
EMI	Electromagnetic Interference
EO	Earth Observation
EOEP	Earth Observation Envelope Program
ESA	European Space Agency
ESL	Expert Support Laboratory
FMI	Finnish Meteorological Institute
FR	Final review
FWF	Freshwater fluxes
GCOS	Global Climate Observing System
GNSS	Global Navigation Satellite System
IAR	Impact assessment report
IASC	International Arctic Science Committee
ICES	International Council for the Exploration of the Sea
ICM	Institute of Marine Sciences
IEEC	Institut d'Estudis Espacials de Catalunya
IPCC	Intergovernmental Panel on Climate Change
ISC	Ice-Sea Contamination
ITT	Invitation to tender
KO	Kick-off
L2OS	Level 2 Ocean Salinity
LSC	Land-Sea Contamination
MFF	Multifractal Fusion
MR	Monthly report
MTR	Mid-term review
MTS	MIRAS Testing Software
MV-TN	Modelling and validation technical note
NS	Nodal sampling
PAR	Preliminary analysis report
PGICs	Peripheral glaciers and ice caps
PM	Progress meeting
PMP	Project Management Plan
PSU	Practical Salinity Unit

PVR	Product Validation Report
RB	Requirements baseline
RD	Reference document
RFI	Radio Frequency Interference
SAR	Synthetic Aperture Radar
SIAR	Scientific and impact assessment report
SMAP	Soil Moisture Active and Passive
SMOS	Soil Moisture and Ocean Salinity
SoW	Statement of work
SR	Scientific roadmap
SSS	Sea Surface Salinity
SST	Sea Surface Temperature
TDP	Technical data package
TN	Technical note
TPM	Third Party Missions
UPC	Universitat Politècnica de Catalunya
VIR	Validation and intercomparison report
VR	Validation report
WCRP	World Climate Research Programme
WP	Work package
WS	Workshop minutes
WWRP	World Weather Research Programme

1 Introduction

1.1 Scope of this document

This document holds the Impact Assessment Report (IAR) prepared by Arctic+ Salinity team, as part of the activities included in the [WP500] of the Proposal (Task 5 from SoW ref. **EOP-SDR/SOW/084-17/DFP**).

The principal objective is to present the impact assessment of the study given the final findings and results.

The assessment of the impact and benefits of the new satellite retrieved SSS v3.1 data developed in this projects is analysed and described. This document also presents a Science Analysis by exploring the application of SSS data to further understand key oceanographic processes in the Arctic.

- Freshwater fluxes from Arctic rivers and Greenland Ice Sheet: this study used river outflow climatology used at NERSC, combined from the ERA-Interim runoffs as input to the Total River Integrating Pathways hydrological model. The Greenland Ice Sheet mass loss will be estimated from the ESA Ice Sheet CCI project and NERSC will distribute freshwater corresponding to the land ice loss from each of the 8 sub-basins down to the 30 largest terminal glaciers around Greenland.
- Freshening of the Arctic: the new SSS products will be used to investigate the decreasing trend in the SSS of the Arctic reported in recent studies, with a specific focus on the anomalous years, its link to the atmospheric variability in the Arctic, and on the associated changes in the Beaufort Gyre dynamics. Further, the potential of the SSS product as a proxy for the variability (temporal) in the freshwater content of the Arctic will be investigated.

1.2 Structure of the document

The IAR is structured as follows:

Section 1 covers the introduction and the description of this document.

Section 2 describes the main SMOS SSS data set and the regions of interest

Section 3 presents the results obtained by data assimilation in TOPAZ4.

Section 4 presents an analysis of the SMOS dataset in the perspectives of freshwater climate and estuarine processes.

Section 5 focuses on the error budget estimation and analysis.

Section 6 concludes and presents future activities.

1.3 Applicable documents

ATBD	Algorithm Theoretical Baseline Document	Arctic+SSS-D3.1-ATBD_v1.0
DUM	Data User Manual	Arctic+SSS_DUM_D1.1_v1r2
RBD	Research Baseline Document	Arctic+SSS_RBD_D1.2_v1r6
SoW	Statement of Work	ref. EOP-SDR/SOW/084-17/DFP
PVR	Product Validation Report	TBD

2 Sea surface salinity impact assessment in the Arctic

The Arctic Ocean is undergoing dramatic changes as it amplifies global warming. The expected effect of the Arctic warming are as follows:

- A warming of the ocean surface in response to warmer winds
- The loss of sea ice, documented by satellite data more than 20 years ago (Johannessen et al. 1999)
- An increased inflow of freshwater, from various sources: from melting sea ice, glaciers and ice sheets and an enhanced hydrological cycle (Carmack et al. 2016). An increased inflow of warm and relatively fresh waters from the Pacific through Bering Strait (Woodgate et al. 2005).
- Enhanced stratification as an effect of the above.

However, even if all the above points towards a general freshening of the Arctic surface waters, the general picture is much more complex: there are regional differences in the Arctic water column structure, with the warm and saline Atlantic waters flowing at the surface of the Barents Sea. The Northern Barents Sea has witnessed an "Atlantification" (Lind et al. 2019) as the retreat of sea ice has also removed the surface sea ice melt freshwater stratification. It is speculated that this Atlantification process may gain the whole Arctic in term. More complexity is added by the natural decadal variability of the Arctic climate. The Barents Sea - again - has also witnessed a decade relatively colder than the previous decade. There are therefore high expectations from a high-quality SSS dataset to document the changes of the Arctic surface waters, with the assistance from an ocean model. Since it is not technically possible to date to process a 10-years Arctic Ocean reanalysis assimilating the SMOS decade within the time frame of this project, the present IAR has fallen back to the following questions:

- Are there benefits of assimilating SSS from SMOS in a 6-months test period of an Arctic reanalysis? (the TOPAZ4 reanalysis of the CMEMS Arctic MFC).
- Are the regional trends of SSS in agreement with the published literature and model results (again from the TOPAZ4 reanalysis)?
- Can independent satellite data measuring indirectly the extent of river plumes (ocean colour) corroborate the SMOS SSS variations?
- How is the error budget of the SMOS SSS dataset with respect to both in situ and SMAP SSS data.

2.1 Data

The project Arctic+ Salinity identified and described some of the most common in situ observations available within the region (ref DUM and RBD). This section aims to present a summary description of those datasets to be used for the evaluation of the impact assessment of using the SSS product produced in this project.

2.2 SSS regional product

Thanks to the ESA funded Arctic+ Salinity project, BEC has developed a regional specific enhanced Arctic SSS product called BEC-L3-SSS-ARCTIC-025km-XXXXXXXX_XXXXXXXX_301.nc.

Description of the new regional SSS product:

- The product will be freely distributed and served at the BEC webpage (http://bec.icm.csic.es/) and at the project webpage (https://arcticsalinity.argans.co.uk).

- The product is distributed in the standard grid EASE-Grid 2.0, which has a spatial resolution of 25Km. The product has a temporal resolution of 9 days (uses 9 days average to compute the map), and the product is served daily.
- L3 products of 3days and 18 days temporal resolution, as well as the L2 product, are also distributed.
- Arctic SSS data is available from 2011-2019.
- The L3 products contain the following data:
    - Sea Surface Salinity (psu)
    - Sea Surface Salinity uncertainty
    - Sea Surface Salinity anomaly: Difference between sea surface salinity provided by SSS field and the annual sea surface salinity provided by WOA 2018 A5B7
    - Flags code:
        - HRE (high_radiometric_error): larger than 1.2 psu for points closer than 150.0 km to the ice edge or coastline;
        - LNM (low_number_of_L2B_measures): less than 4 L2B orbits;
        - LNMCORR (low_number_of_L2B_measures_in_spatial_correction_field): less than 50 L2B orbits good_quality
        - (GQ): None of the above.

2.3 Description of different test regions

This project selected three different test areas to validate the Assimilation experiment of the first Arctic+ dataset. These test areas should not be confused with those for product validation in the PVR. The Requirement Baseline Document (RBD) collected a thorough rationale for the selection of each of these testing regions. These regions were:

1. The Beaufort Sea in the Canadian Basin
2. Nordic Seas, from the Greenland Scotland Ridge (GSR) to about 80˚N
3. Northern North Atlantic (50˚N to GRR)

In all three regions salinity controls the surface ocean circulation and there is a strong salinity variability due to the freshwater (FW) fluxes.

3 Results of the Impact Assessment

3.1 Sea surface salinity assimilation in TOPAZ

The different versions of the SSS product have been assimilated in the TOPAZ4 system (identical to the official Arctic reanalysis in CMEMS) and comparison to independent in situ salinity data has proven that the assimilation of the V3 SSS was beneficial.

3.1.1 Visual inspection of the V3 SSS data

The Figure 3.1-1 below shows monthly averaged SSS from the V3.1 product assimilated from July to December 2016.

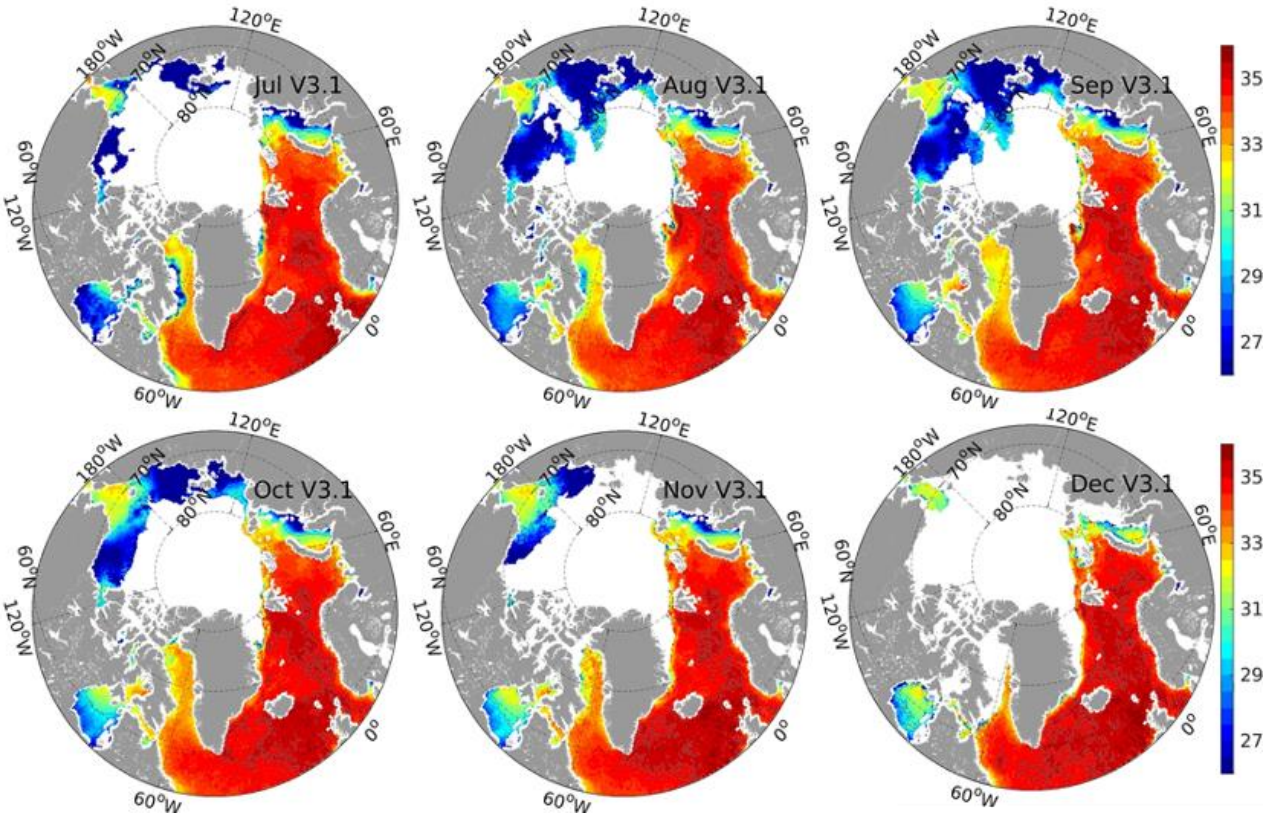

Figure 3.1-1 Monthly averaged SSS from the V3.1 from 9-days composites. A qualitative assessment shows that the following features of interest are respected:

- Atlantic waters (>35 psu) occupy the expected regions of the Norwegian Basin and Barents Sea.
- The SSS is well below 30 psu in marginal seas in Summer.
- The Norwegian coastal current is fresher in July, corresponding to the maximum snow melt in Norway.

3.1.2 Experimental Setup

TOPAZ4 is a coupled ice-ocean data assimilative system, using the HYCOM-CICE model at a resolution of 10 km over the whole Arctic and the Ensemble Kalman Filter (EnKF) running 100 dynamical members to assimilate all available ocean and sea ice observations jointly (Xie et al. 2017). The atmospheric forcing fields are from the ECMWF. The hydrographic properties of TOPAZ4 have been validated in Lien et al. (2016) and Xie et al. (2017). The system provides both the near real time forecast and reanalysis products of the Copernicus Marine Services (CMEMS) Arctic Monitoring and Forecasting Center (Arctic MFC).

Two parallel runs of the TOPAZ4 reanalysis system (Xie et al. 2017) have been integrated for the year 2016 assimilating the SMOS data in addition to all other data sources available (altimeter data, SST, sea ice concentration, sea ice drift, T/S profiles, sea ice thickness). The assimilation has been carried out on a weekly basis as is practiced in the TOPAZ4 reanalysis, the SMOS L4 9-days composite data valid for the day of the analysis has been assimilated. The model error terms arise from uncertainties in surface forcing fields and receive random spatially correlated perturbations with a spatial correlation radius of 250 km, in particular:

a) The wind forcing (of amplitude standard deviation about 10 m/s)

b) The air temperature (of standard deviation 3K)

c) The precipitations (of standard deviation of 100% using a lognormal probability law).

No uncertainties are assumed in the river inputs (both runs will use the same river inputs).

The EnKF used the L4 SSS uncertainty estimates provided by WP300 and increased them to account for representation error (i.e., the mismatch of the model and observation grids and the time difference between the satellite passage and the EnKF assimilation time). The errors standard deviation are therefore increasing for lower salinity values following the function adjusted by Xie et al. (2019) as in Eq (1):

$$\boldsymbol{\sigma}_{obs} = \text{Max}\,(\boldsymbol{\sigma}_{product},\ 0.6\ \text{psu} + 6\ \text{psu}\ /(1+\exp((S-16)/5))), \qquad (1)$$

with S being the observed SSS expressed in psu. $\boldsymbol{\sigma}_{product}$ the error specified in the SSS product (zero if not specified, like in the V2 product). This means that the observation errors are larger in the V3 than the V2 data, but only for saline waters.

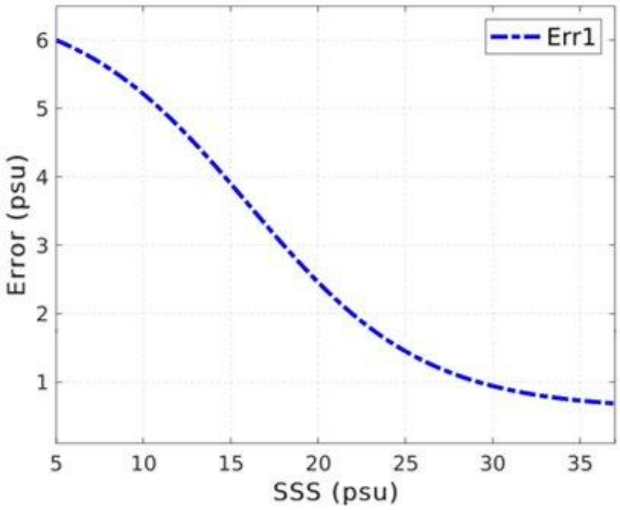

Figure 3.1-2: Observation error used for assimilation as a function of the salinity observation.

The EnKF data assimilation has run with and without SSS in a fully multivariate mode, following the EnKF principles, so that the ocean 3D variables and the sea ice variables in the vicinity of SSS observations have also been updated according to the background covariances from the 100-members ensemble. Reversely, the assimilation run without SSS does as well increment the model SSS as multivariate updates of the other assimilated observations (ice concentration, hydrographic profiles and SST typically).

Three experiments are summarized in Table 3.1.2-1:

Table 3.1.2-1 Overview of the three data assimilation experiments of the Observing System Experiment. Experiment V2 may appear as J2 in some graphics below, although they are the same experiment.

Exp.	Start date	End date	SSS	SSS Error	Other Obs.
0	-	-	*no*	-	*Yes*
V2/J2	6th Jul	28th Dec	*V2 (9d)*	*Eq. 1*	*Yes*
V3.1	6th Jul	28th Dec	*V3.1 (9d)*	*Eq. 1*	*Yes*

3.1.3 Data assimilation diagnostics

The good health of the EnKF data assimilation system is monitored by comparing the innovation statistics to the background and observation errors at each assimilation step. This results in the time series given in Figure 3.1-3. The mean innovation should ideally remain close to zero, except in cases of model biases or observation biases (the assimilation system does not discriminate one from the other). The Root Mean Square (RMS) innovation should ideally be equal to the sum of background errors ($\boldsymbol{\sigma}_{ens}$, or "ensemble spread") and observation errors ($\boldsymbol{\sigma}_{obs}$).

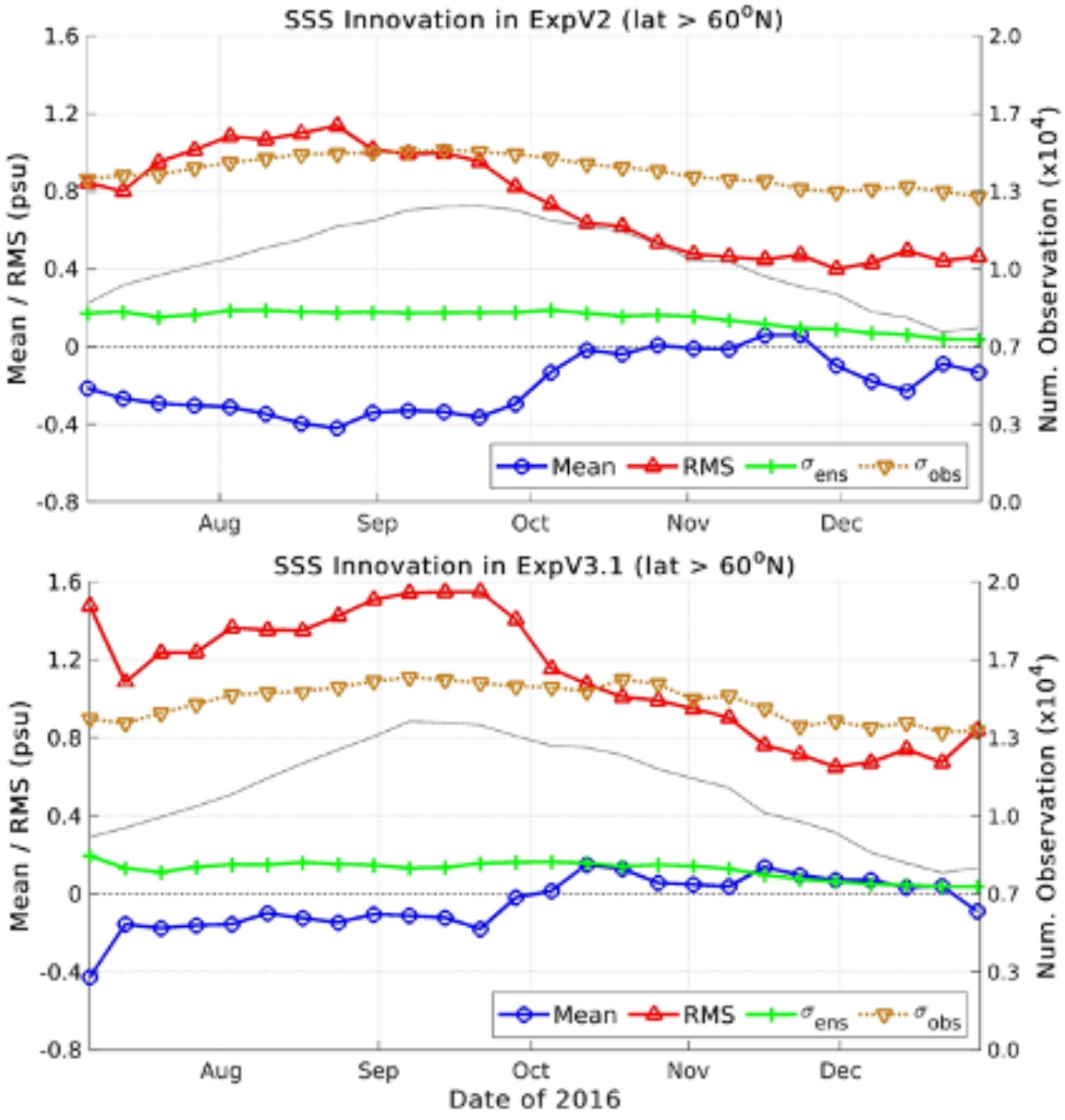

Figure 3.1-3 Innovations (observations minus model) statistics for the V2 data (marked "J2", top) and the V3 data (bottom). Mean is the bias, RMS the root mean square innovation, σ_{ens} the ensemble spread and σ_{obs} the

observation errors. The gray line shows the number of observations assimilated, which varies inversely with the sea ice mask.

Figure 3.1.3 shows that the bias is 0.2 psu smaller in V3 than V2, but that the RMS of innovations is 0.5 psu larger in V3. This is likely due to the well-known "double penalty" effect: since the V3 product has a higher effective resolution, the position errors increase the innovation RMS compared to the smoother V2 product.

For both the V2 and V3 SSS data, the RMS of innovations is commensurate with the sum of background (ensemble) and observations errors. This proves that the EnKF has not diverged and that we can be confident in the rest of the evaluation. The background error is about 1/5th of the observation error, which is a sign of excessive confidence in the model with respect to the evaluation in Xie et al. (2019), but is a "safe" operating mode for the EnKF: it warrants small assimilation shocks and the stability of the assimilative model.

3.1.4 Qualitative evaluation of the data assimilation increments

We investigate how the assimilation of different SSS products influence the reanalysed SSS, as well as the SST due to multivariate ensemble covariances.

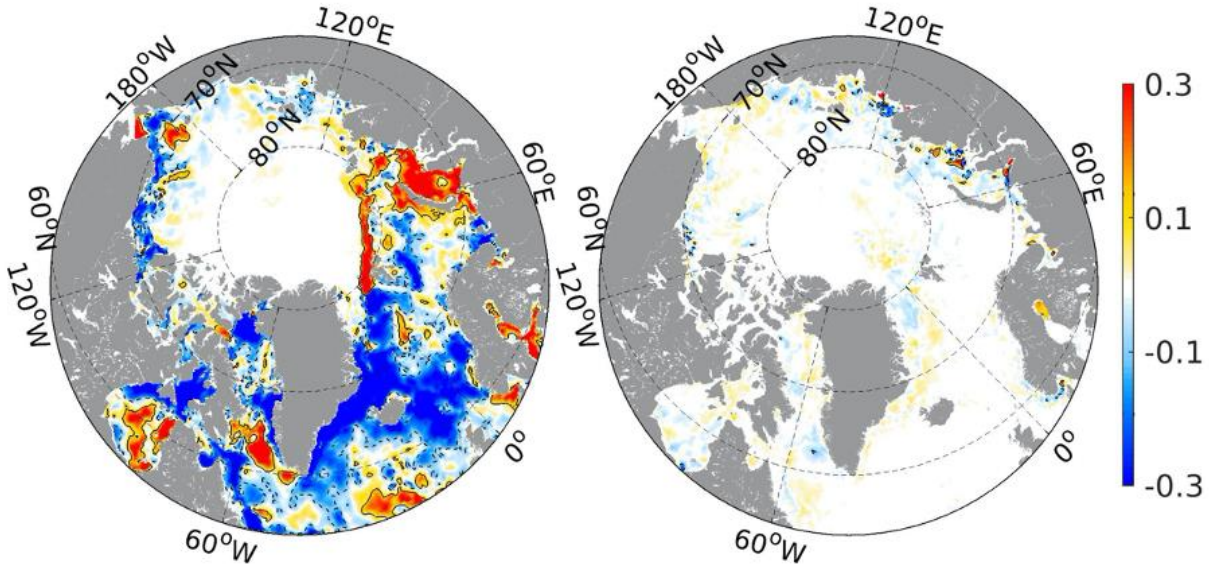

Figure 3.1-4 Increments of SST (left) and SSS (right) from Exp0, the control reanalysis without SSS. Solid (dashed) lines are 0.1 (-0.1) deg and psu respectively, averaged over July – December 2016.

Figure 3.1-4 shows how the assimilation of all other data sources but SSS increment the model SST and SSS. The SSS increments are small and on small spatial scales and will be ignored in the following comparisons. They are caused by the multivariate ensemble covariances when assimilating sea ice concentrations, SST, in situ profiles and altimeter data.

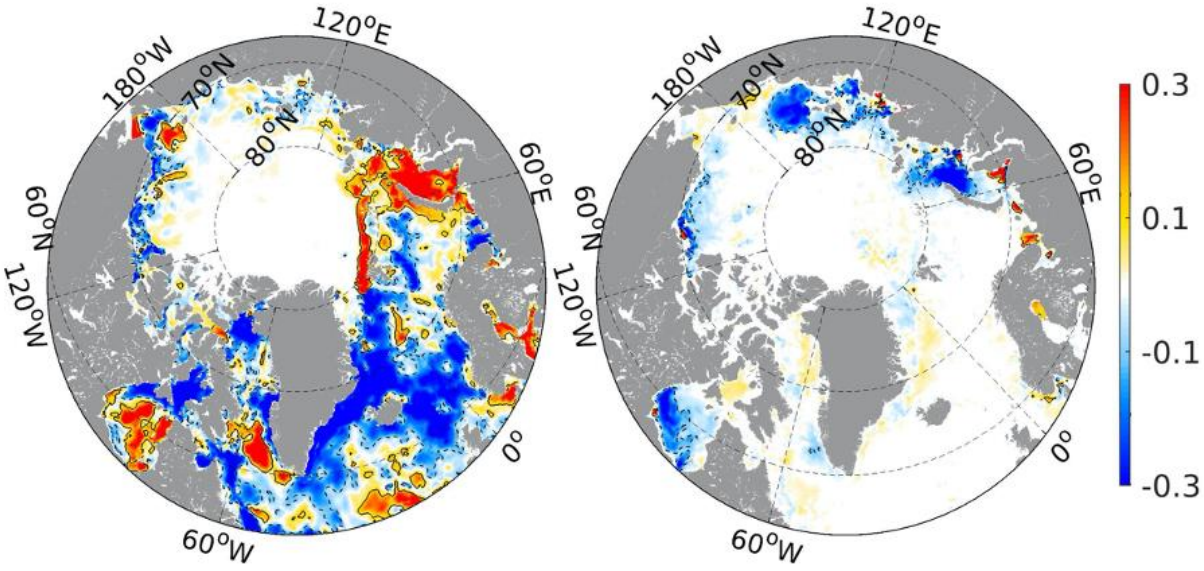

Figure 3.1-5 Same as above from Exp2, the reanalysis assimilating V2 SSS.

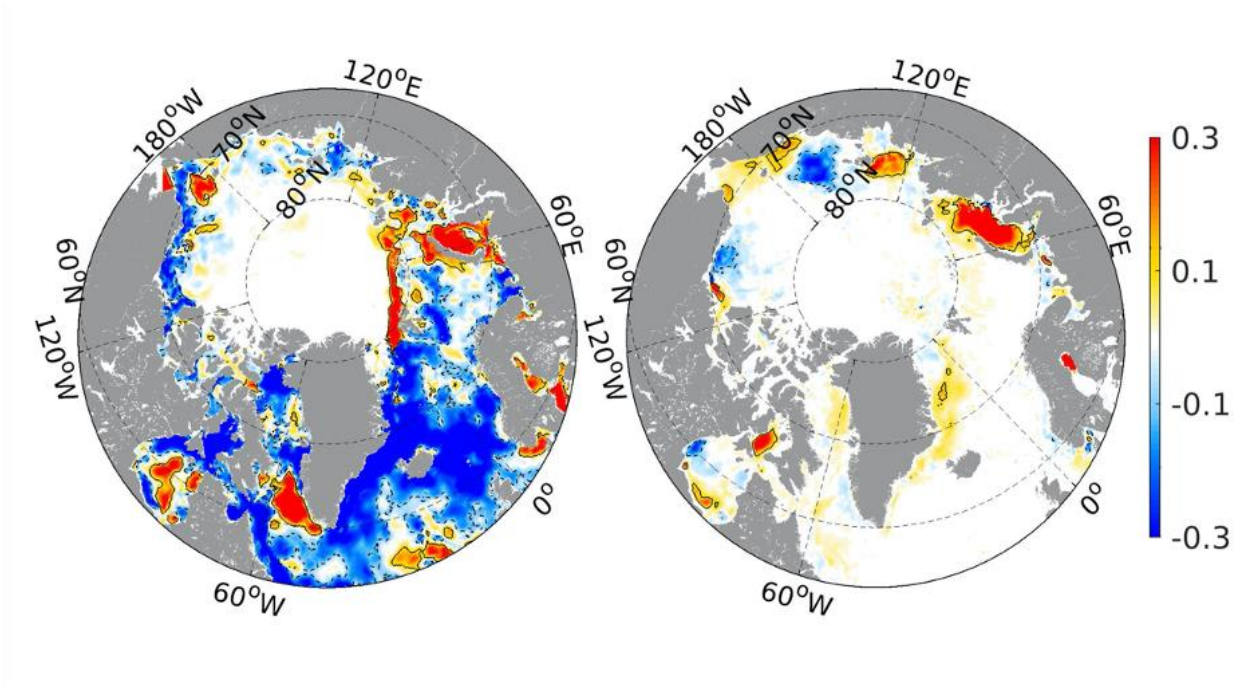

Figure 3.1-6 Same as above from Exp3.1, the reanalysis assimilating V3.1 SSS.

The comparison of the SSS increments related to V2 and V3.1 products show that the V3.1 product increases the model SSS in the Kara Sea and Laptev Sea while the V2 product decreases it. Both V2 and V3.1 products decrease the SSS in the Beaufort Sea except in the Mackenzie river delta, where the V3 product increases the SSS. Unfortunately, we do not have access to independent data that could

corroborate whether these changes are for the better or the worse. Data on the Russian Shelves would be particularly precious in this case.

In the Greenland Seas, the V2 product decreases the SSS near the coasts and increases the SSS further offshore, while the V3 product increases the SSS both near-coast and offshore.

The V2 product increases the SSS in the Norwegian Coastal Current, while the V3.1 product freshens it, especially in the Skagerrak.

The SST increments are mostly identical in all three runs.

3.2 Validation against independent data

The validation period went from July to December 2016. An overview of the profiles, data sources and regions is given in below Figure 3.2-1.

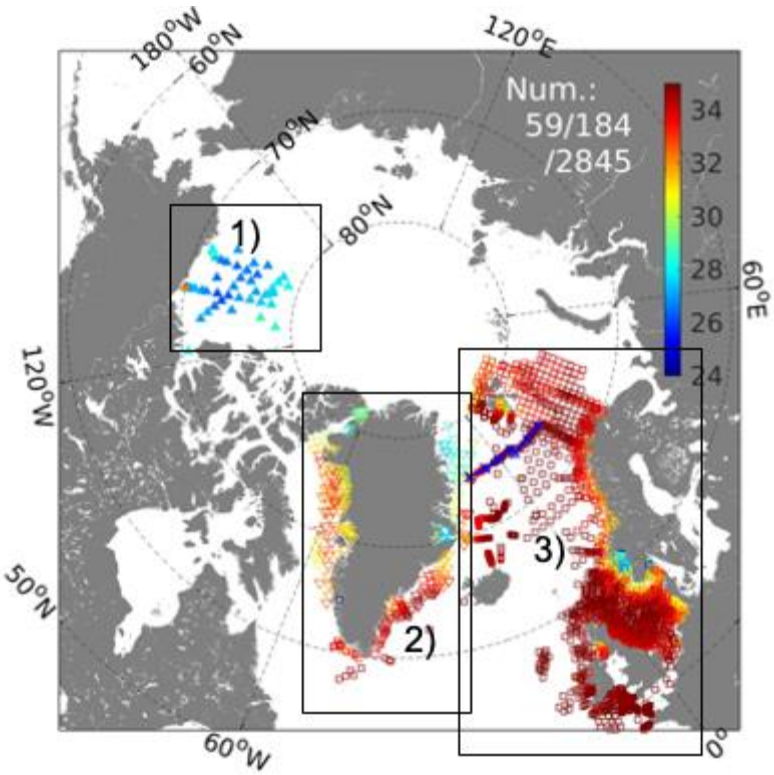

Figure 3.2-1 Overview of independent in situ salinity profiles used for validation. Colour indicates salinity averaged over the top 8 meters. 1) Beaufort Gyre BGEP, WHOI, 2) Oceans Melting Greenland, NASA, 3) ICES Nordic Seas.

3.2.1 Beaufort Gyre

59 profiles are available from the BGEP moorings in the period of interest. The scatterplots of TOPAZ versus in situ data (averaged over the upper 8 meters) are shown in Figure 3.2-2.

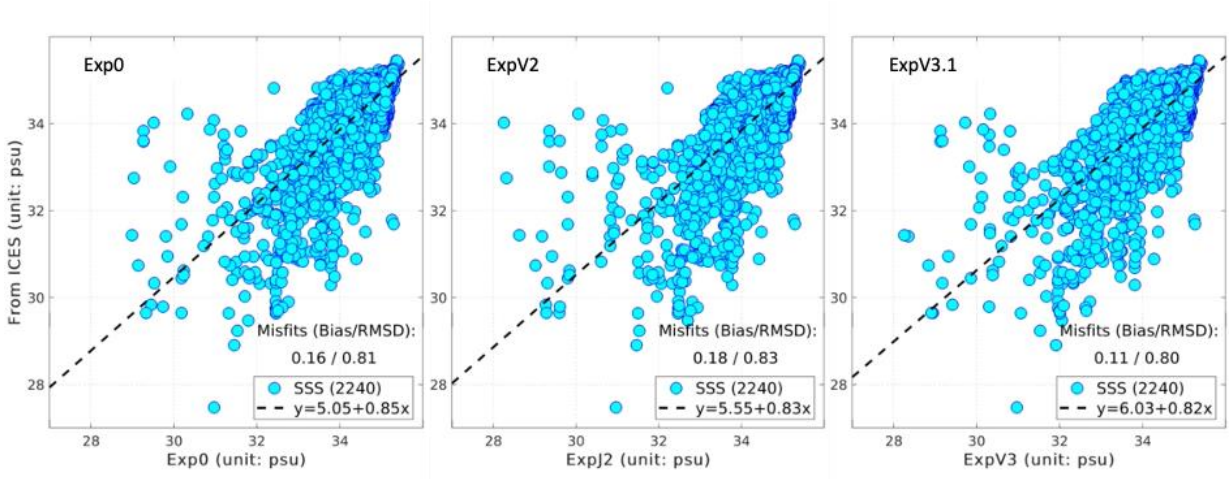

Figure 3.2-2 Scatterplots of in situ against model SSS interpolated at the mooring locations in the Beaufort Sea.

The TOPAZ4 model has a severe saline bias in the Beaufort Gyre, which decreases by assimilating both products: 15.9%(V2) and 28.6% (V3). The RMS differences also decrease: 10.8%(V2) and 16.2% (V3). These basic statistics both prove the V3 SSS product advantageous over V2.

We however note that the very low regression slope indicates rather poor model skills in this area, as expected from Xie et al. (2019).

3.2.2 Greenland Seas

The OMG data from NASA holds 163 profiles with salinity data in the upper 8 meters in the second half of 2016.

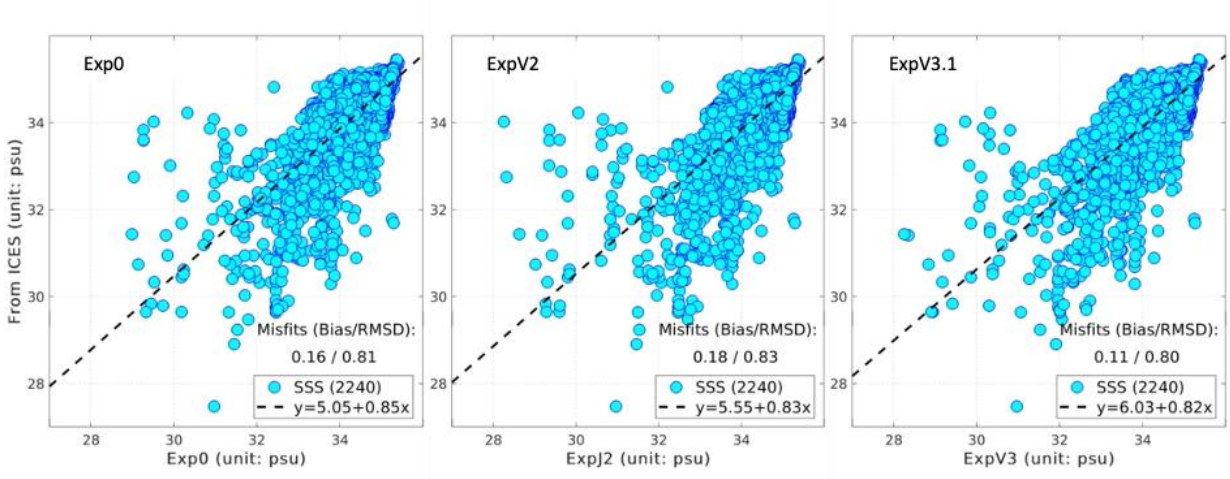

Figure 3.2-3 Same as above for the Greenland Seas, using the OMG campaigns from NASA.

TOPAZ4 exhibits a saline bias at the locations of the OMG data, which decreases by assimilating the V3 product by 17.3%. The RMSD also decreases by 8.2%. The assimilation of the V2 data does not seem to improve the statistics and if anything, rather points to a degradation. The OMG data thus shows a unique advantage of the V3 product.

3.2.3 Nordic Seas

The ICES data collection covers the Celtic Sea, the North Sea, the Norwegian Sea and well into the Barents Sea. The data coverage is much more extensive than in the Beaufort Sea or Greenland Sea with 2240 profiles.

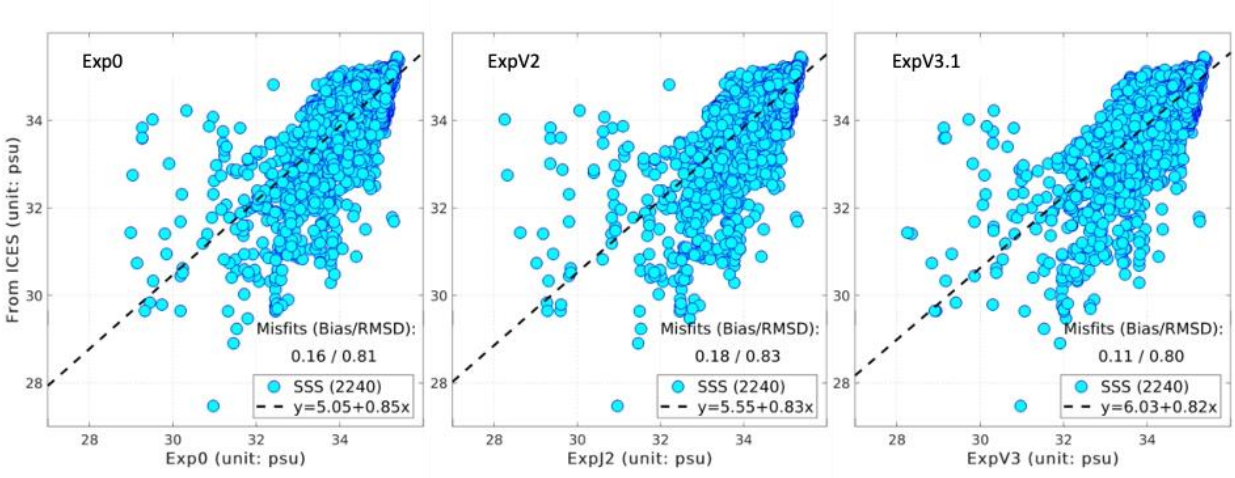

Figure 3.2-4 Same as above for the Nordic Seas, using the ICES data collection.

The comparison indicates a saline bias of the TOPAZ4 system. The V2 data increases slightly the errors, but V3 does reduce the saline bias (by 0.05 psu, consistent with previous validation results in Xie et al. 2017, their Figure 9, attributed to insufficient vertical resolution in the model). The RMSD is not improved but not degraded by the V3 product. This region therefore shows another relative advantage of the V3 product over V2.

3.2.4 Visual consistency check

Several areas are not well covered by in situ observations and deserve a qualitative verification of the effect of assimilating SSS data.

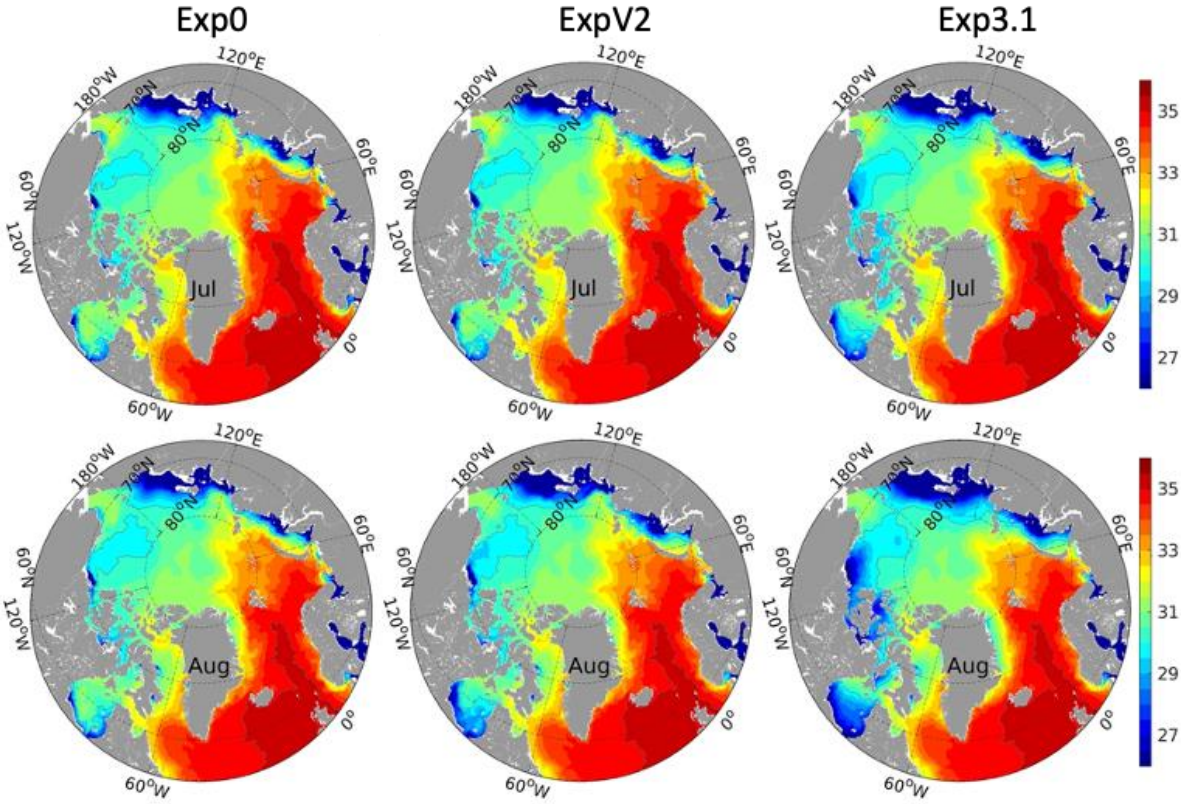

Figure 3.2-5 Monthly averaged SSS from the three assimilation runs: no SSS (left), V2 (middle column) and V3 (right). The first row is the month of July and the second row August.

Figure 3.2-5 shows the impact of assimilation in the summer months, the first two months after the start of the OSE. Fresher waters are observed near the coasts, particularly when assimilating the V3 product. This is visible in the following areas: the Norwegian Coastal Current, the East Greenland Sea near Denmark Strait and the South of Hudson Bay.

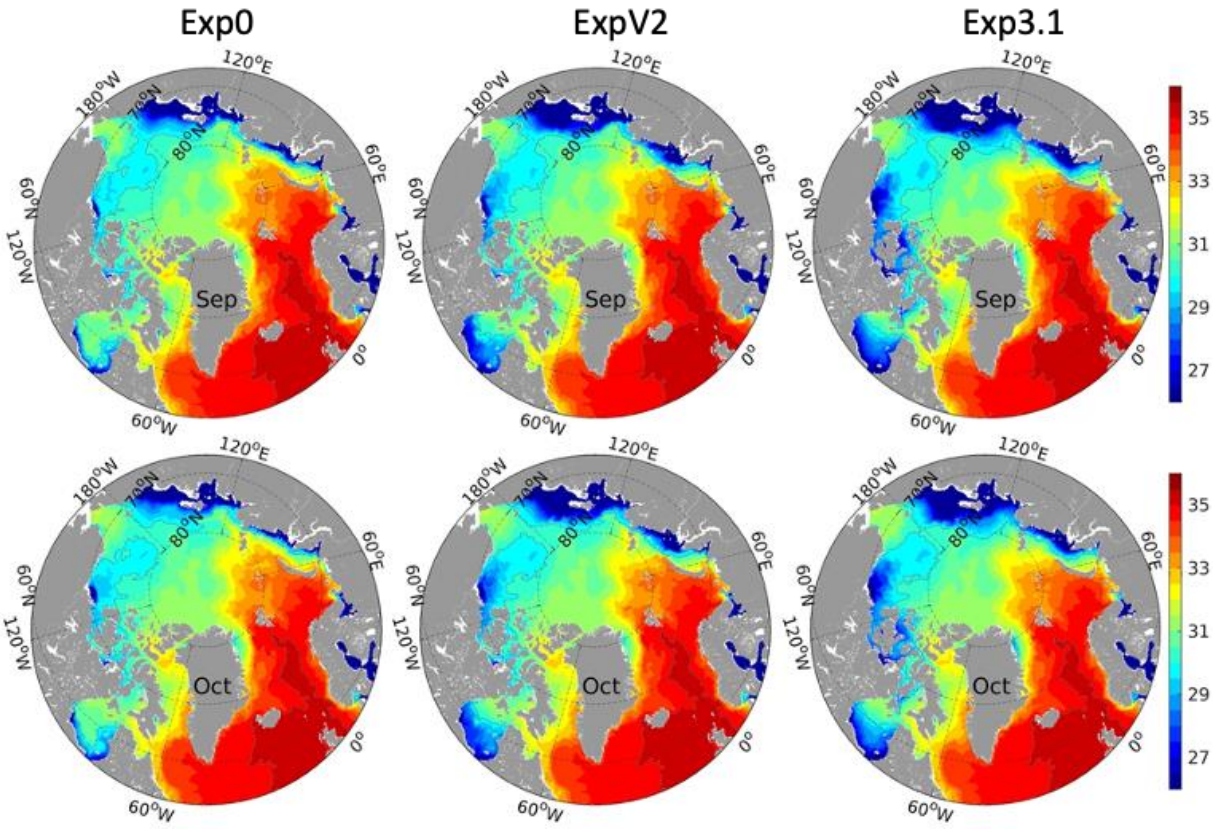

Figure 3.2-6 Same as above for September and October 2016.

Figure 3.2-6 shows the progression of the differences in the 3rd and 4th month following the start of the experiment. The freshening of the Beaufort Sea continues both in the V2 and V3 assimilation experiments. The V3 experiment however differs from the V2 experiment in the East Greenland Sea where the area of freshwater appears wider than in V2. The extent of Atlantic waters appears similar in all three runs.

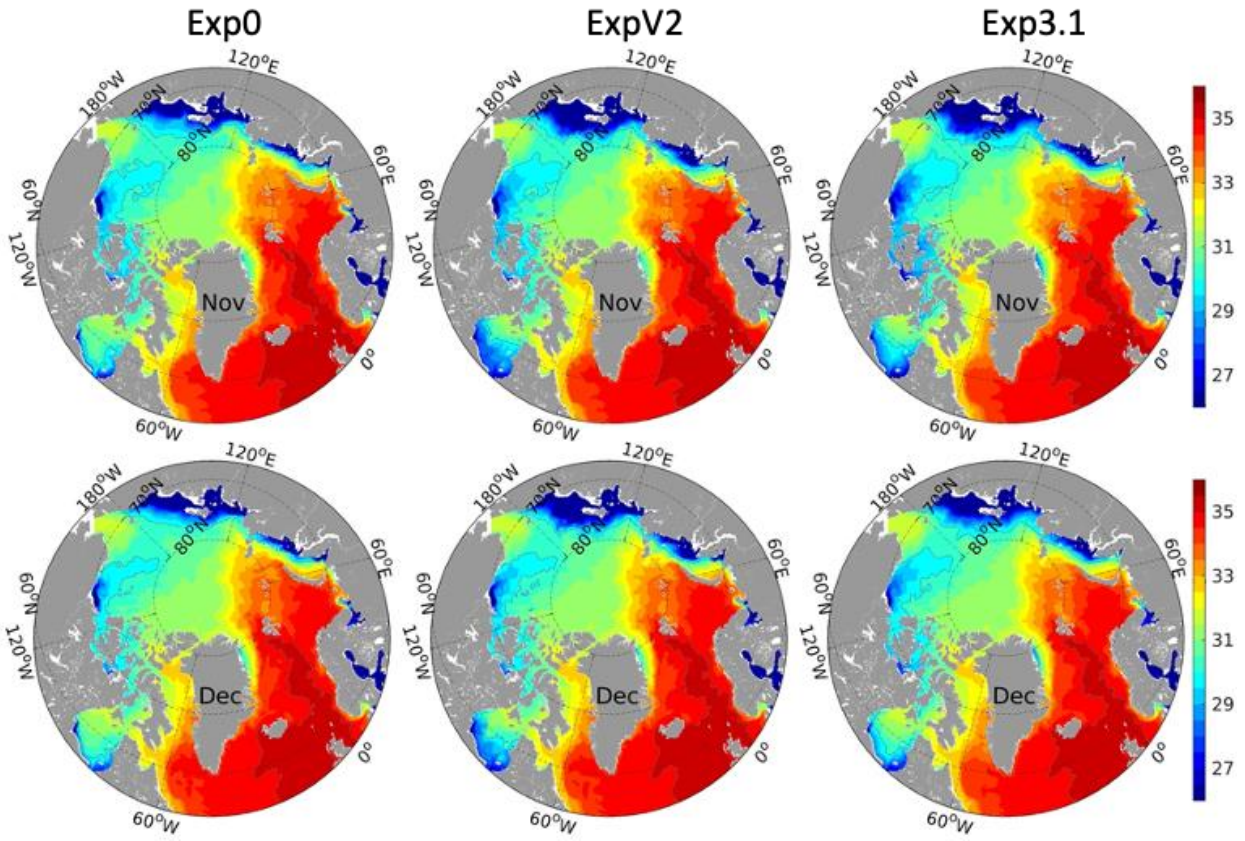

Figure 3.2-7 Same as above for November and December 2016.

The end of the Fall shows the return to higher SSS in all three runs, as expected. One difference however appears in the Southern Kara Sea that is related to a known model setup error: the river Ob discharge was mis-located to the West of Yamal Peninsula, resulting in excessive freshwater there. Only the assimilation of the V3 product does correct the - human - mistake there.

Contrary to what happened in August, the Hudson Bay is fresher when assimilating the V2 than the V3 product, indicating a different seasonal cycle in the two products. There are unfortunately no in situ measurements to qualify the products in the Hudson Bay.

3.3 Characterization of different ocean features dependent on Sea surface salinity product

The liquid freshwater content (FWC) of the water column has been computed from the three aforementioned TOPAZ4 assimilation runs and calculated using the standard formula (Serreze et al. 2006, Proshutinsky et al. 2009) in Eq. (2):

$$\mathrm{FWCL} = \int_{z2}^{z1} \frac{[Sref - S(z)]}{Sref} dz,$$

Eq. (2)

Where the reference salinity value Sref is taken at 34.8 psu and the vertical integral is computed on all waters fresher than Sref.

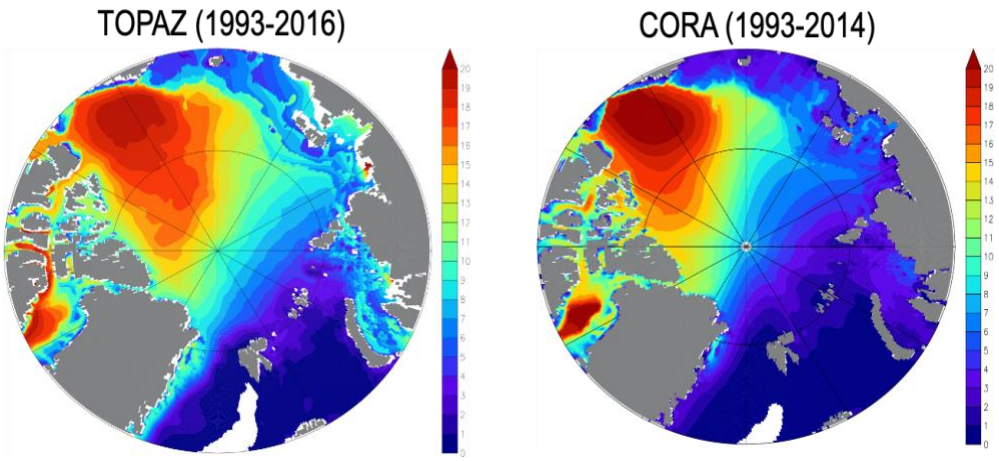

Figure 3.3-1 Comparison of modelled TOPAZ4 (Exp0, left) FWC against the estimate from interpolated in situ observations (the Coriolis objective analysis reprocessing, CORA, right). Values are expressed in meters. Note that the time averaging period is slightly different between the two.

Figure 3.3-1 shows a broad agreement between the model and observed FWC with a maximum FWC in the Beaufort Sea except for a broader area in TOPAZ toward the interior of the Arctic but a thicker FWC from in situ observations. Note that these maps are climatological and provide a general impression of the TOPAZ4 system versus observations rather than an assessment of the particular year 2016.

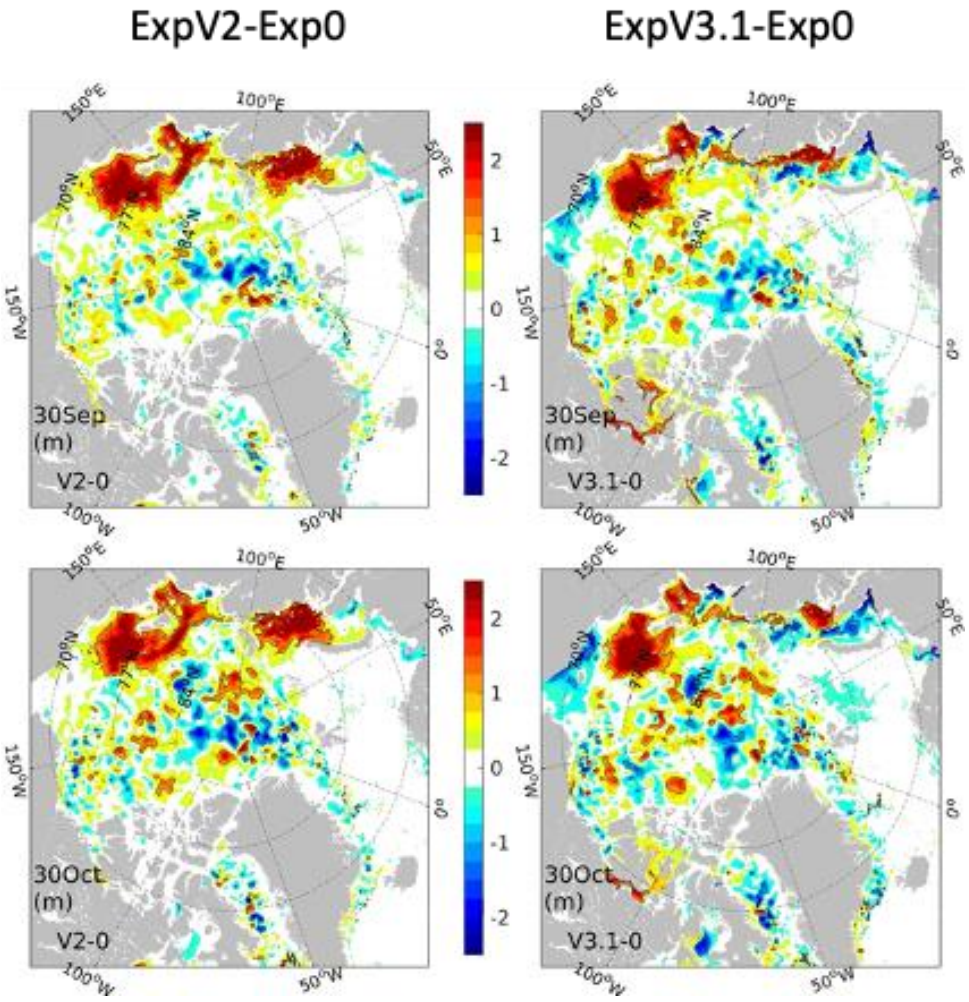

Figure 3.3-2 Maps of Freshwater content (FWC) differences relative to the control experiment. Top line: September, bottom: October. Solid (dashed) lines are +1 (-1) meter difference.

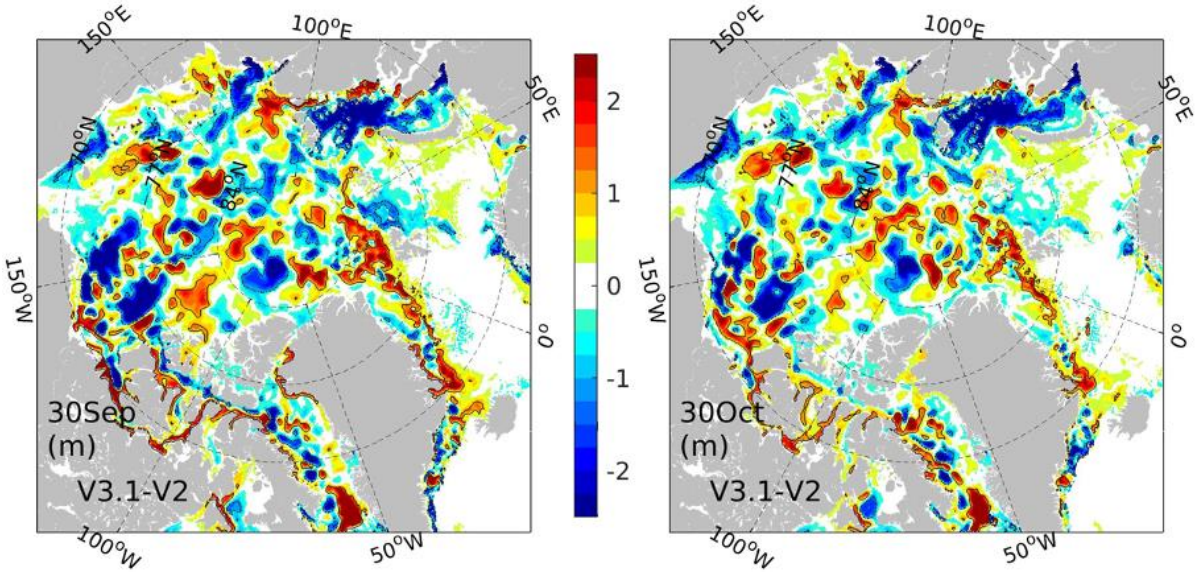

Figure 3.3-3 Maps of Freshwater content (FWC) difference between ExpV3.1 and ExpV2. Left: September, Right: October. Solid (dashed) lines are +1 (-1) meter difference.

Figure 3.1-3 exhibits the differences between the SSS assimilation runs and the official Exp0 reanalysis, thus showing the impact of the V2 (left) and V3.1 (right) SSS products on TOPAZ4. Both products lead to a significant increase of the FWC after assimilating SSS on the Siberian Shelf (especially in V2, but less so in V3.1). This is true in September when the salinity is at its lowest. The increase of FWC along the Siberian shelf is not expected from the comparison to climatology in Figure 3.31 but the interannual changes in Siberian river runoff are very large and the river Lena had larger than usual discharge in 2016 (cf. EU H2020 NUNATARYUK project). The large river discharge alone can explain such large increase compared to the FWC climatology, since the model rivers are climatological.

The differences from V2 to V3.1 are more patchy than the differences to V0 but the reduction of FWC in the Kara Sea is consistent with the positive SSS increments seen in Figure 3.16.

A deepening of the FWC max in Beaufort Sea is also visible in V3 and in the Canadian Archipelago (closer to the coast).

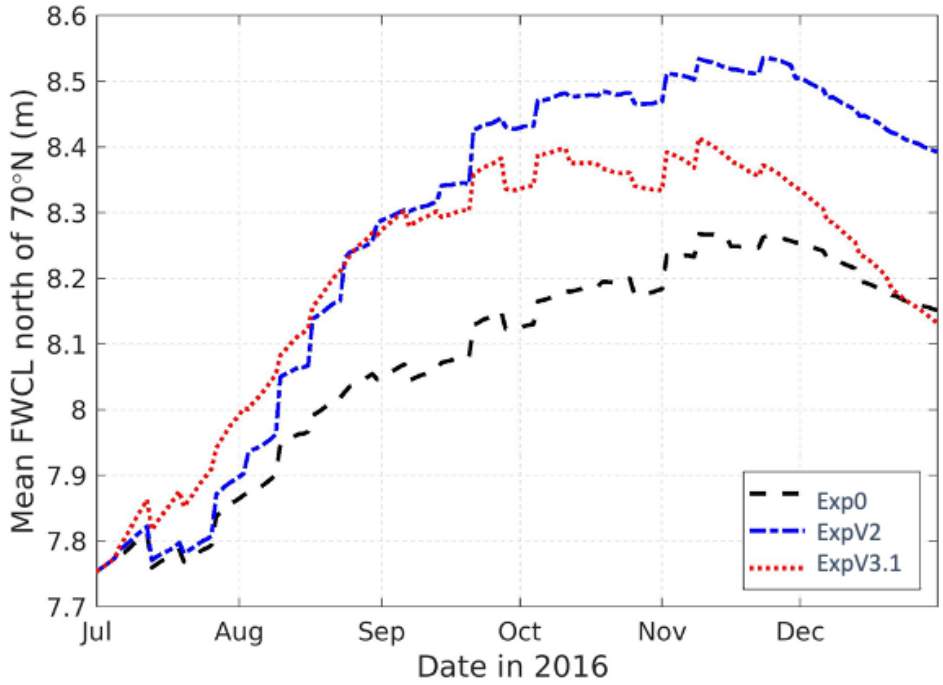

Figure 3.3-4 Time series of daily pan-Arctic (North of 70N) Freshwater content layer thickness (in meters) in the Official run and the V2 and V3 SSS assimilation runs.

An Arctic-wide integral of the FWC estimates from the three model runs is presented in Figure 3.3-4, revealing stark differences of seasonal cycle between the three runs that can be fully attributed to the SSS data assimilation.

The impact of weekly data assimilation cycles is visible as instantaneous jumps in the three time series. These data assimilation artefacts were already present in the official Exp0 reanalysis due to the multivariate increment assimilation of data sources other than SSS. They are roughly of the same order of magnitude with the assimilation of SSS (generally below 10 cm of FWC) but are occasionally larger in the run assimilating V2 data in August. The main changes between the three runs concern mostly the aspect of the seasonal cycle:

1. The timing of the maximum FWC comes earlier with assimilation of V3 data (both with earlier increase and earlier decrease of FWC) but is synchronous in the official run and in the run assimilating V2 data. It is not possible with the data at hand to tell whether this is a change for the better or the worse.
2. The FWC grows thicker with assimilation of SSS data, in particular with the V2 data with an offset of 30cm. This is mostly related to the differences on the Siberian Shelves (**Error! Reference source not found.** - left)
3. Since there is not enough ground truth data in 2016, the above comparison can only be qualitative. Relative to Exp0, the two assimilation runs both increase the area-averaged freshwater thickness.

4 Scientific Analysis

4.1 Impact of mass loss from the Greenland Ice Sheet

This section provides a sensitivity study of the Greenland Sea SSS to the addition of Greenland Ice Sheet mass loss. The study uses the TOPAZ4 model in free run, without any data assimilation. This provides an initial result towards a complete freshwater budget of the Arctic.

In practice, the time series from the 8 drainage basins are fitted by linear regression and the slope of the regression is converted in a freshwater flux, which needs to be partitioned into estuaries along the coast of Greenland. Table 3.4.1 indicates the correspondence between the 8 drainage basins of the GrIS CCI study and the 30 associated terminal glaciers. The split of freshwater between the glaciers within the same basin is equal for simplicity.

Table 3.2.4-1 List of 30 main glaciers selected in this study.

Drainage Basin	No.	Glacier
GS01 (23.5 Gt/yr)	L1	Petermann Gletscher
	L2	Humboldt Gletscher
	L3	Ryder Gletscher
	L4	C.H. Ostenfeld Gletscher
	L5	Hagen Bræ
	L6	Academy Gletscher
GS02 (2.9 Gt/yr)	L7	Nioghalvfjerdsfjorden
	L8	Zachariae isstrøm
	L9	Storstrømmen
GS03 (45.3 Gt/yr)	L10	Kangerlussuaq Gl.

	L11	Kong Christian 1V glacier
	L12	Daugaard-Jensen Glacier
	L13	Waltershausen Gletscher
GS04 (36.2 Gt/yr)	L14	Helheimgletscher
	L15	Ikertivaq Glacier
	L16	Gyldenløve Fjord
	L17	Tingmiarmiut Fjord
GS05 (22.7 Gt/yr)	L18	Eqalorutsit Killiit Sermiat
	L19	Sermiligaarssuk
	L20	Ukaasorsuaq
GS06 (38.4 Gt/yr)	L21	Narsap Sermia
	L22	Kangiata Nunaata Sermia
	L23	Frederikshåb Isblink
GS07 (30.7 Gt/yr)	L24	Jakobshavn Isbrae
	L25	Sermeq kujalleq glacier
	L26	Rink Isbrae Gl
GS08 (52.7 Gt/yr)	L27	Upernavik Isstrøm

	L28	Kong Oscar Gletscher
	L29	Hayes Gletscher
	L30	Heilprin Gletscher

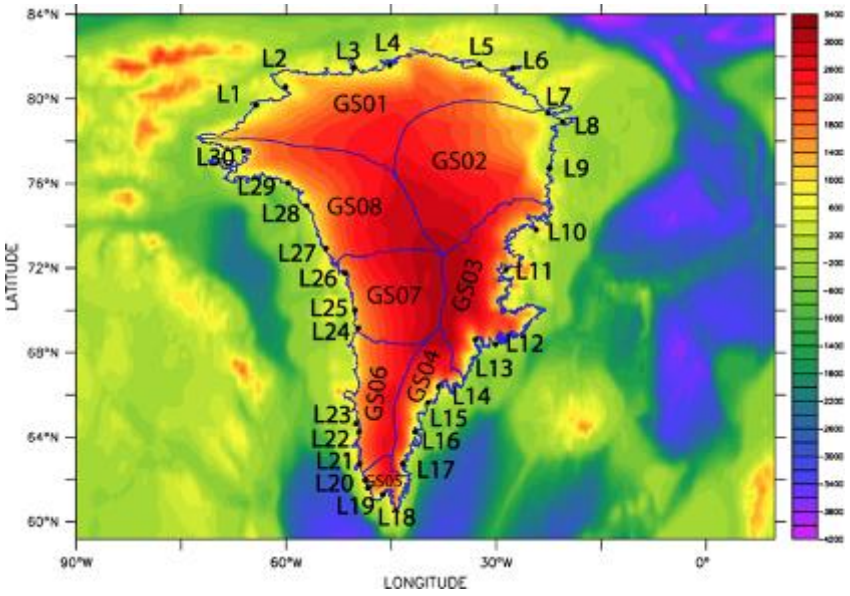

Figure 4.1-1 Topography of Greenland and its surrounding regions. Locations of 30 selected glaciers (L1 - L30) detailed in Table 3.4.1 are shown as black dots, while the polygons shown in blue represent the 8 drainage basins (GS01 - GS08) defined by the GrIS CCI.

The gravity variations in the 8 drainage basins are shown in Figure 4.1-1 for reference. Once the GrIS mass loss is added to the freshwater discharge into the TOPAZ system, the total discharges increase as shown in Figure 4.1-2 below. The freshwater discharges doubles on average all around Greenland. Note that the seasonal cycles of the mass loss and the surface mass balance included in the ERA-Interim-TRIP part are different, although this is not shown here.

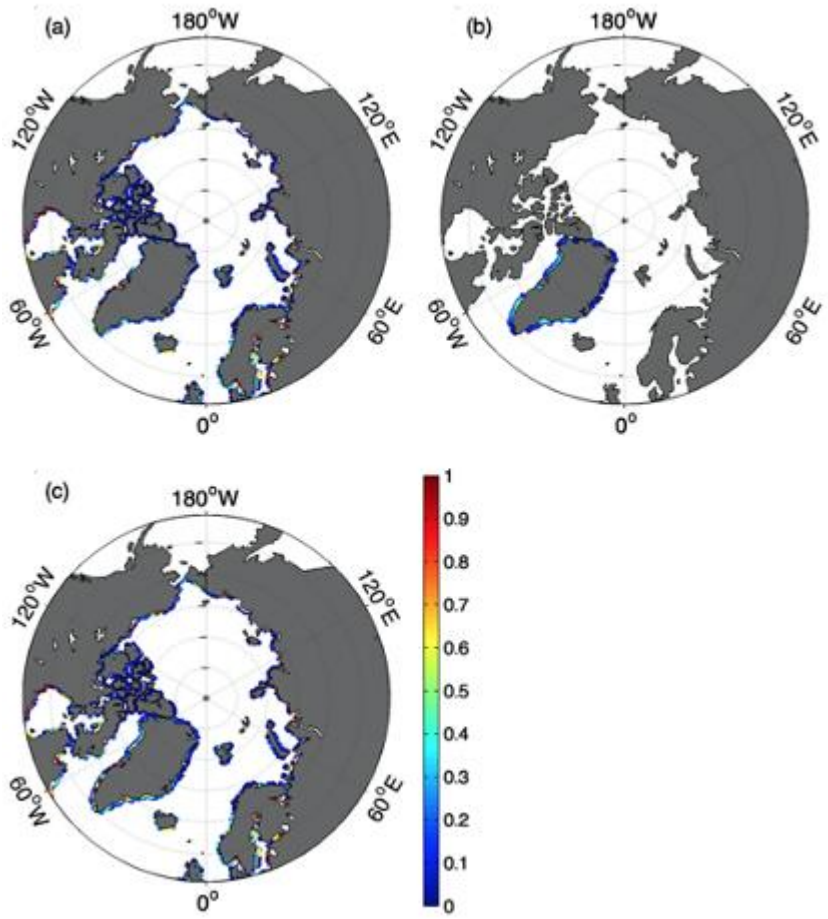

Figure 4.1-2 Freshwater flux (10^{-7} m/s) model input data: (a) Total Runoff Integrated Pathways - with ERA-Interim climatology runoffs, (b) Greenland Ice melt, (c) Combined.

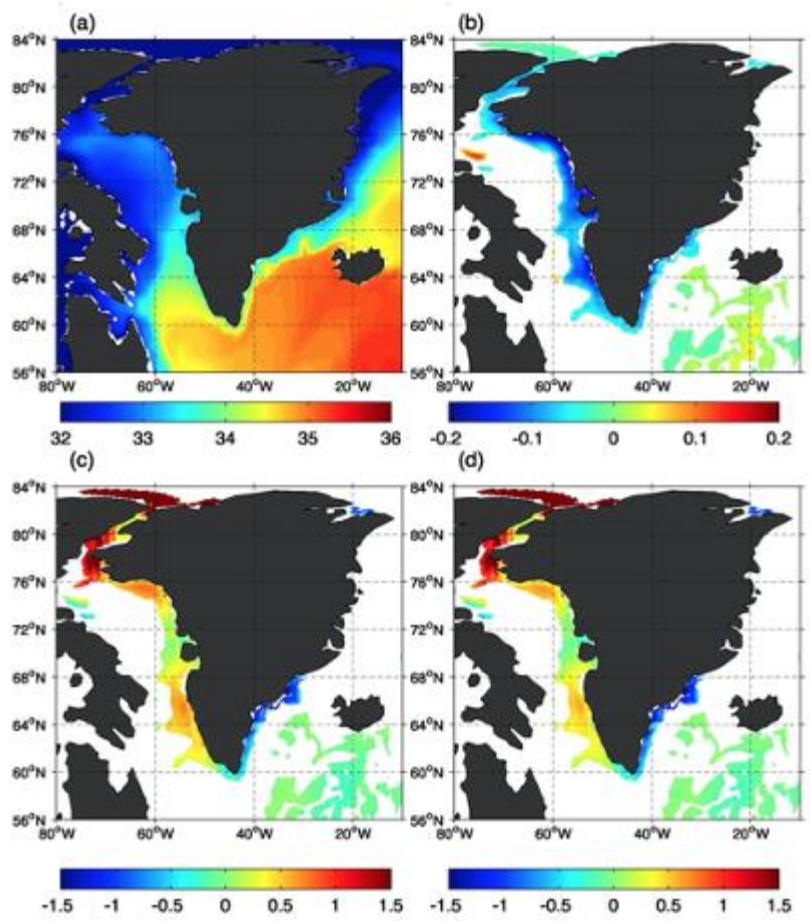

Figure 4.1-3 (a) Climatology (2006-2014) of upper ocean salinity (0-50m; in psu) in the Greenland region from TOPAZ4 (run with Greenland mass loss). (b) Difference in the mean (2006-2014) salinity (0-50m; psu) of the TOPAZ control run and the TOPAZ Greenland run. Non-significant differences are masked. Difference between the mean (2006-2014) salinity of: (c) CORA and TOPAZ (control run); (d) CORA and TOPAZ (Greenland run). Non-significant grid points from panel b are masked in both panels c and d.

We perform a sensitivity analysis on the TOPAZ free run (without data assimilation) in order to quantify the effect of freshwater flux from Greenland Ice melt on the model results. The model is integrated twice with and without the GriS mass flux for a period of 9 years (2006-2014 included). The time-averaged difference in Figure 4.1-2(b) shows a freshening all along the West Greenland coast by 0.2 psu as a result of the added freshwater from Greenland, although no significant difference on the East Greenland side. With reference to the assimilation study (Figure 3.1.6), 0.2 psu is larger than the time-averaged assimilation increments from the SSS assimilation run. This should be expected as the addition of the GrIS mass loss doubles the freshwater fluxes from Greenland, which is a stronger deviation than the TOPAZ4 ensemble spread can reach with only uncertainties in atmospheric forcing. A new reanalysis that includes GrIS mass loss and SSS assimilation is now ongoing for the December 2021 CMEMS release, also with higher vertical model resolution. Further by comparing with *in-situ* observations we assess the improvements in the model results when the contribution of freshwater flux from Greenland Ice melt is incorporated as a model input. Figures 3.4.3 c) and d) show that the saline model biases to the West of Greenland are slightly reduced by the addition of the GrIS mass loss. More remote areas in the Irminger

Sea show an increase of the surface salinity, which are an indirect dynamical effect of the freshening of the Greenland coastal currents: as the salinity gradients around Greenland increase, the circulation of Atlantic waters South of Iceland increases as well, thus bringing more saline waters into the Irminger Sea. A more detailed study of the dynamical effects of the Greenland mass loss would be beneficial to the interpretation of SSS signals in the model output and in the SMOS data.

4.2 Correlation study between SSS and coloured detrital matter (CDM) in the Arctic rivers plumes

At this point we exploit the capability of newly produced SMOS SSS Arctic+ product in conjunction with standard optical products, to assess the relationship between sea surface salinity and colored detrital matter in two large Siberian rivers: the Lena and Yenisei-Ob plumes (Black boxes in Figure 4.1.1). Mixing of fresh river waters and saltier sea waters in the Siberian shelves of the Laptev and Kara Seas forms large river plumes with a typical thickness of ~10 m (Harms & Karcher, 1990). The area of the riverine plume extension depends on the amount of freshwater flowing into the sea and the conditions of the wind forcing, and the vertical water structure of Kara and Laptev Seas is strongly stratified caused mainly by the great rivers discharges.

The large river discharges carry higher loads of dissolved organic matter and suspended matter entering the Arctic Ocean. The ocean subsurface optical parameter we use is the level 3 8-days, 25 km resolution estimate of the colored dissolved and detrital organic materials absorption coefficient at 443 nm (CDM). This product is developed, validated, and distributed by ACRI-ST GlobColour service using MODIS AQUA sensor data (http://www.globcolour.info/).

Mean SMOS and Globcolor maps during the ice-free summer season (Jul-Sep) from 2016 to 2019 (Figure 4.21) display the spatial SSS and CDM variability of the Kara and Laptev Seas with the extension of fresh and turbid plume waters. The Kara Sea is saltier (30-34 psu) than the Laptev Sea (26-30 psu) and both Seas are affected by plume waters (fresher than 27 psu) that spread from Ob and Yenisei Rivers to the Kara Sea and from Lena River to the Laptev Sea more than 400 km northward from the river mouths (Heim et. al, 2019).

The river plumes are also evident in CDM maps associated with a higher concentration of dissolved and detrital organic matter, with typical values of 0.9 m^-1 at the river mouth and descending to 0.1 m^-1 at the edge of the plume extension delimited by 27 psu. The delimitation of 27 psu to delimit the river plume waters is selected to depict the area where SSS and CDM covary and in line with previous studies characterising these plumes (Polukin, 2019 and Gonçalvez-Araujo et al. 2015).

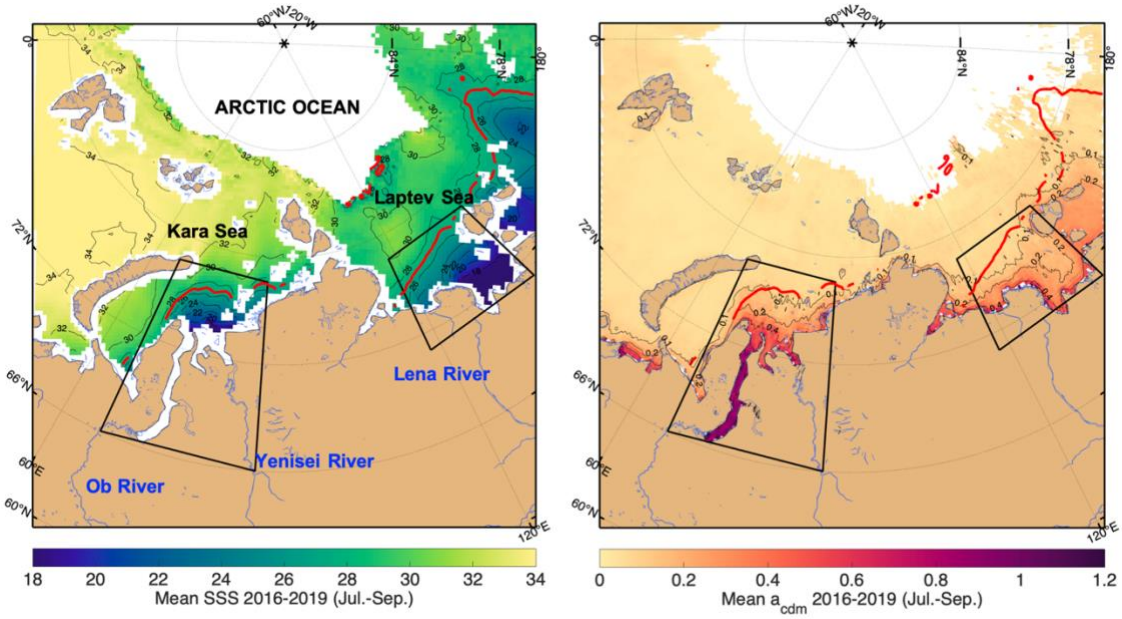

Figure 4.2-1 Left: Mean SSS for months July-September and years 2016-2019 with the isohaline of 27 psu in solid red line. Right: Mean CDM. Black boxes indicate the selected areas of study: Yenisei-Ob rivers plume (66-88°E, 66-76.6°N) and Lena river plume (118-140°E, 71-76.6°N).

The river plumes extension present an interannual variation in SSS (Figure 4.2-2). Note for example how the plume of Yenisei and Ob rivers extend further north and westward in July 2017 than in 2016. We can see another example of the interannual variability in the Lena plume, extending northward in September 2018 and westward in September 2019. The CDM images are affected by cloud coverage, and missing points are evident in the CDM monthly mean (Figure 4.2-3). Notice that there is no optical data in October as the area is fully affected by clouds. In general, CDM covary with salinity as expected but we see an interannual variation on the quantity of CDM along the plume, for example, lower quantity is found in July 2018 than in July 2019.

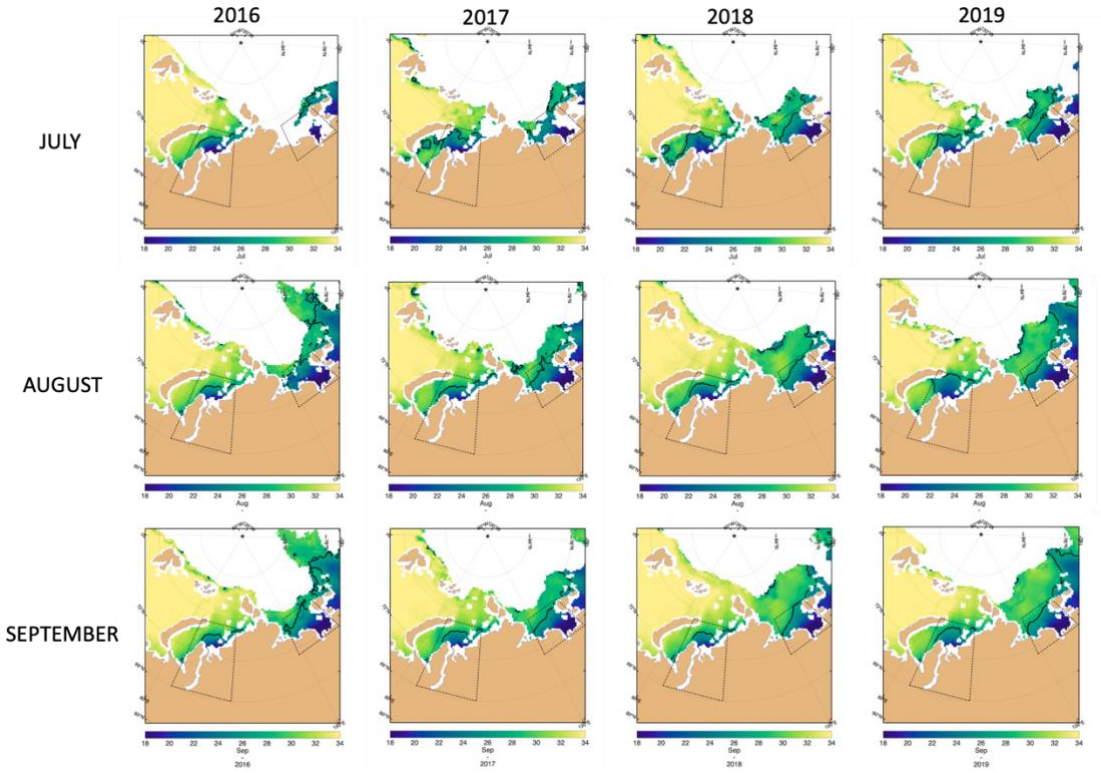

Figure 4.2-2 The monthly means of SMOS SSS maps for 2016-2019. The mean monthly isohaline of 27 psu in solid black line.

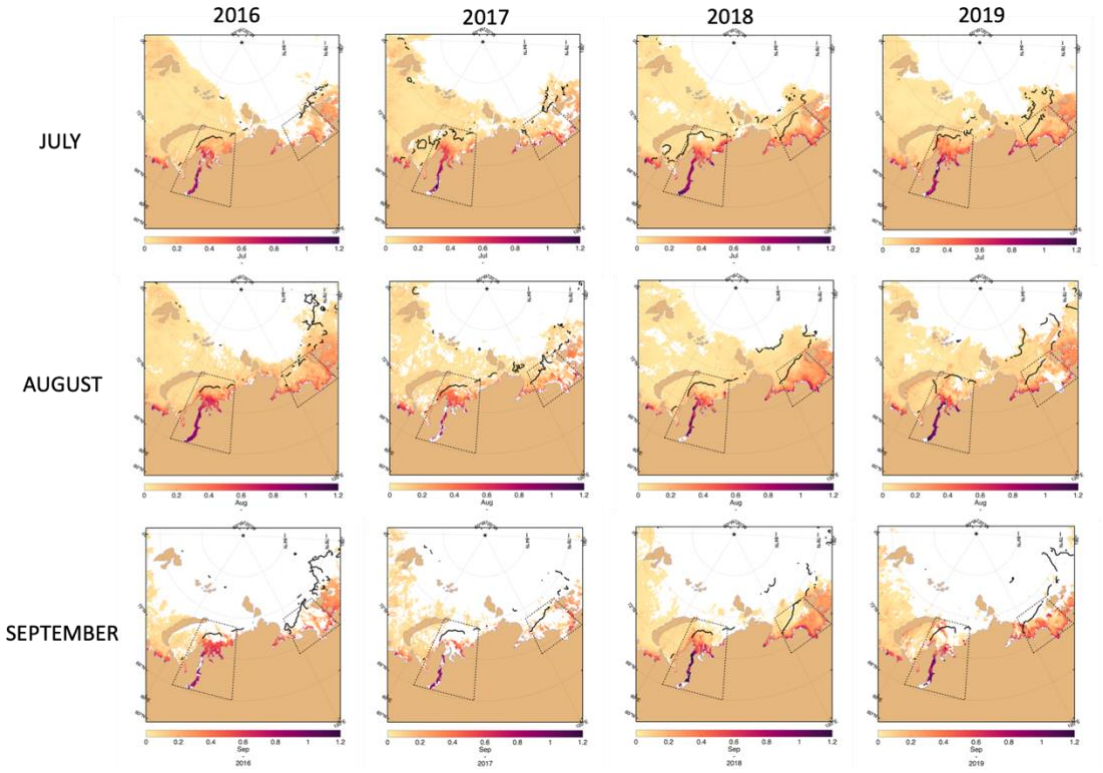

Figure 4.2-3 The monthly means of CDM for 2016-2019. The mean monthly isohaline of 27 psu in solid black line.

Another factor to take into account in this area is the presence of sea-ice, salinity signatures linked to ice formation and ice retreat are expected. The time series of mean sea ice fraction from OSISAF inside the study areas (

) show how the area is deeply affected by sea-ice coverage along the year. Overlap of SSS retrieved in the area and sea ice fraction happen when part of the box has ice and part of the box is ice-free. We can retrieve SSS from July to October (ice-free months) but it might be possible that some of the freshwater may be coming from local sea ice melting and not only from river discharge However, the analysis of isotope characteristics of freshened surface layers in the Kara Sea have revealed that its volume is composed of river water directly mixed with saline water (Dubinina et al., 2017a, 2017b). During late summer and autumn, large river discharge determines the freshwater balance, while the contribution to sea ice melt is negligible (Osadchiev et al., 2021).

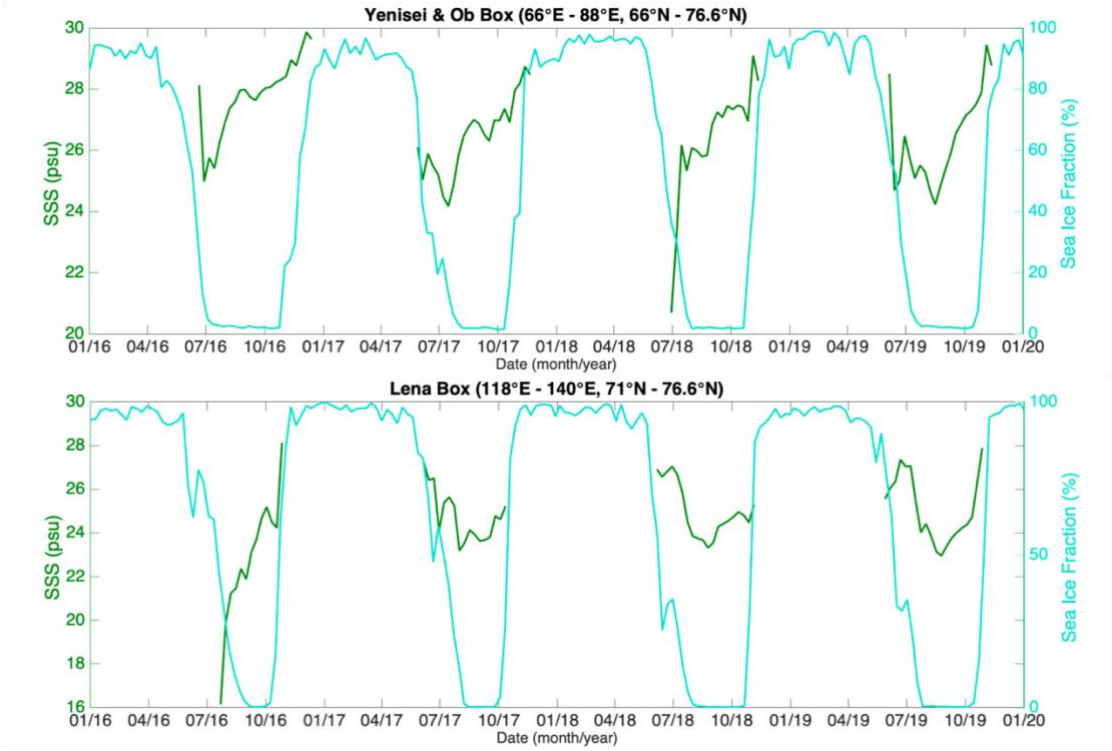

Figure 4.2-4 Time series of the mean SMOS SSS (green) and the mean sea ice fraction (cyan) computed at Yenisei and Ob box (top) and Lena box (bottom).

A negative linear correlation between salinity and the detrital matter has been reported using in-situ and satellite data in the Lena river plume area (Gonçalvez-Araujo et al. 2015, Kubryakov et. al, 2016), and along other river estuaries as in the Baltic Sea (Ferrari and Dowell, 1998), in the Amazon plume (Korosov et al. 2015, Fournier et al. 2015), the Gulf of Mexico (Hu et al. 2003), the Mississippi River plume (Del Castillo and Miller, 2008) and Changjiang river in the East China sea (Bai et al. 2013).

Using the new SMOS SSS v3.1, we obtain a negative linear correlation between mean SSS and CDM inside the river plume boxes (Figure 4.2-5) for years 2016 to 2019, with correlation coefficients of -0.85 for the Lena Box and -0.65 for the Yenisei Box. As expected, fresher riverine waters are associated with higher quantities of dissolved and particulate matter, and saltier marine water corresponds with a lower concentration of CDM.

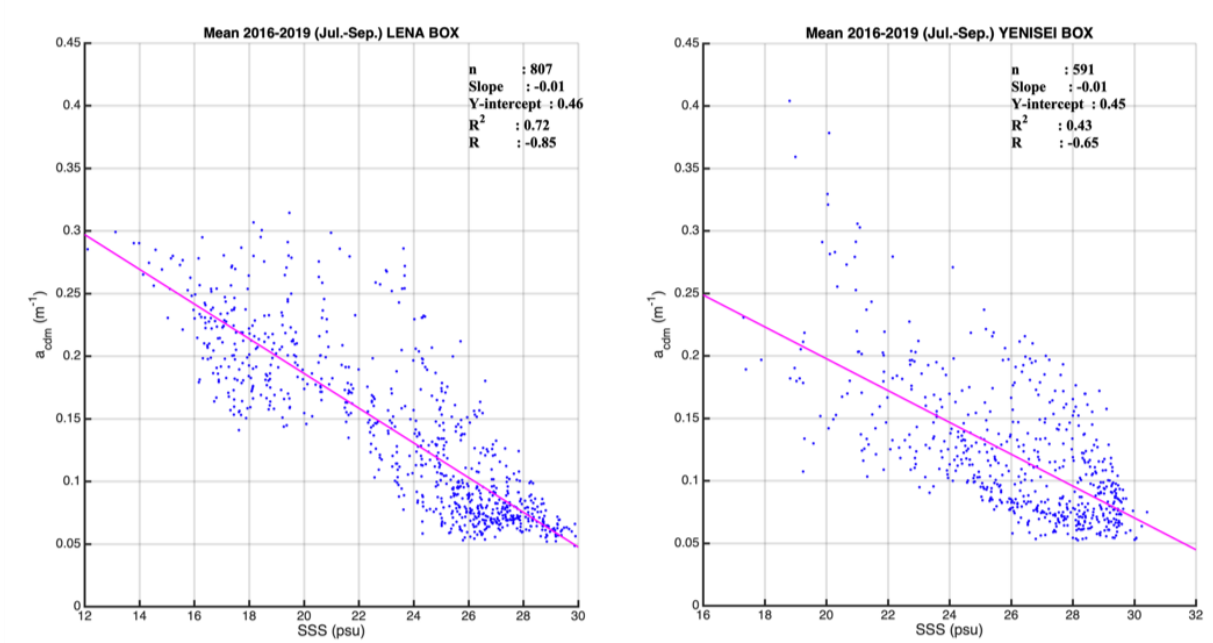

Figure 4.2-5 Mean CDM as a function of mean SMOS SSS over summer months (July to September) of 2016-2019 inside Lena river plume box (left) and Yenisei-Ob rivers plume box (left). The magenta solid line represents the linear regression.

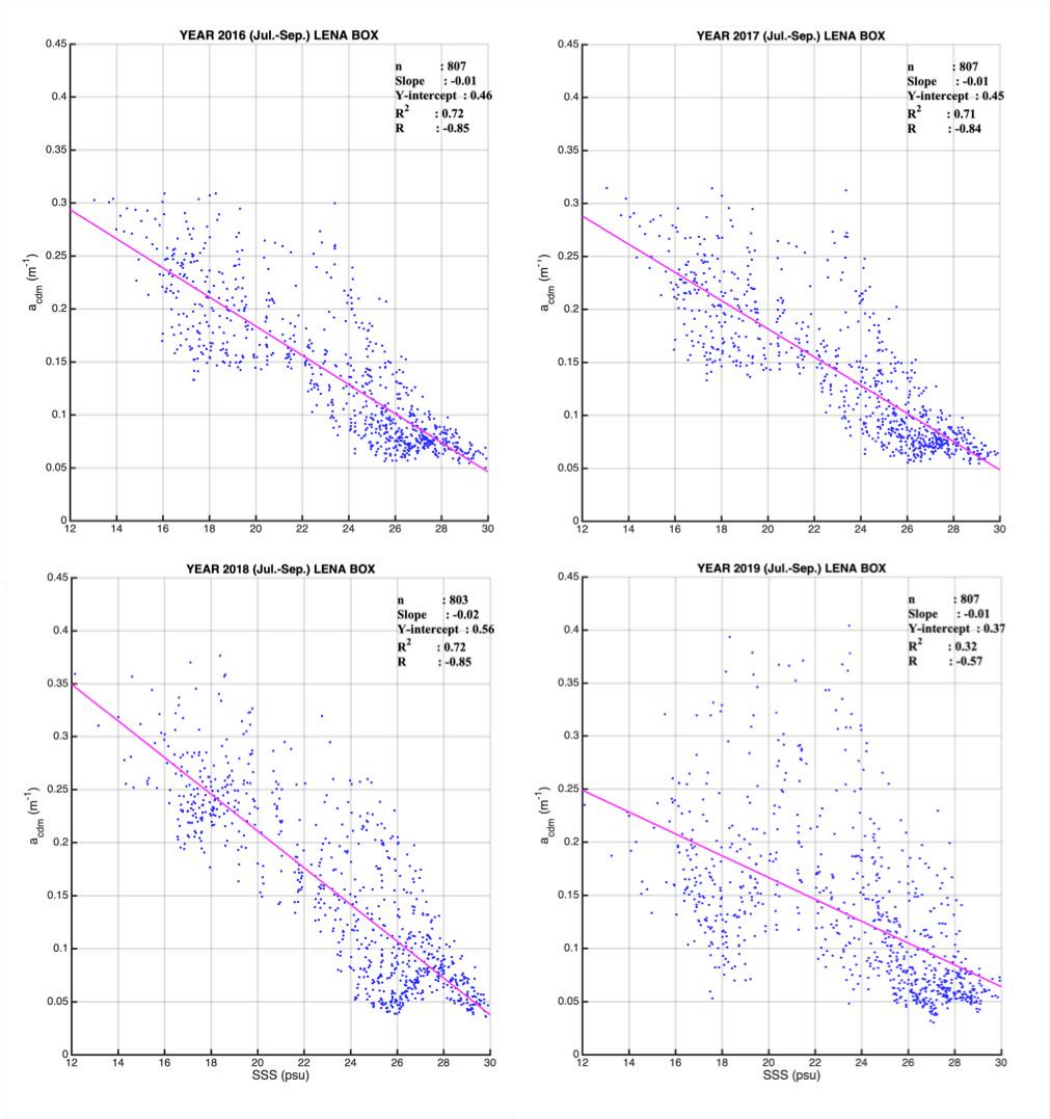

Figure 4.2-6 Interannual variability of mean CDM as a function of mean SMOS SSS over summer months (July to September) for years 2016 to 2019 inside the Lena river plume box. The magenta solid line represents the linear regression.

There exists some interannual variation for the years 2016-2019 in both the Lena and Yenisei Boxes (Figure 4.2-6 and Figure 4.2-7 respectively). Inside the Lena box, the correlation coefficients are -0,85, -0,84, and -0.85 for years 2016, 2017, and 2018, but descend to -0.57 the year 2019 as the scatter plot is more spread due to lower CDM values associated with fresher salinities, compared to the rest of the years. The Ocean Colour data in the year 2019 may be of poorer quality because some corrections are applied with two years of delay (A. Mangin, pers. comm.).

The overall agreement of CDM and SSS is better in low-salinity waters than the comparison of SSS against in situ profiles as seen in Xie et al. (2019).

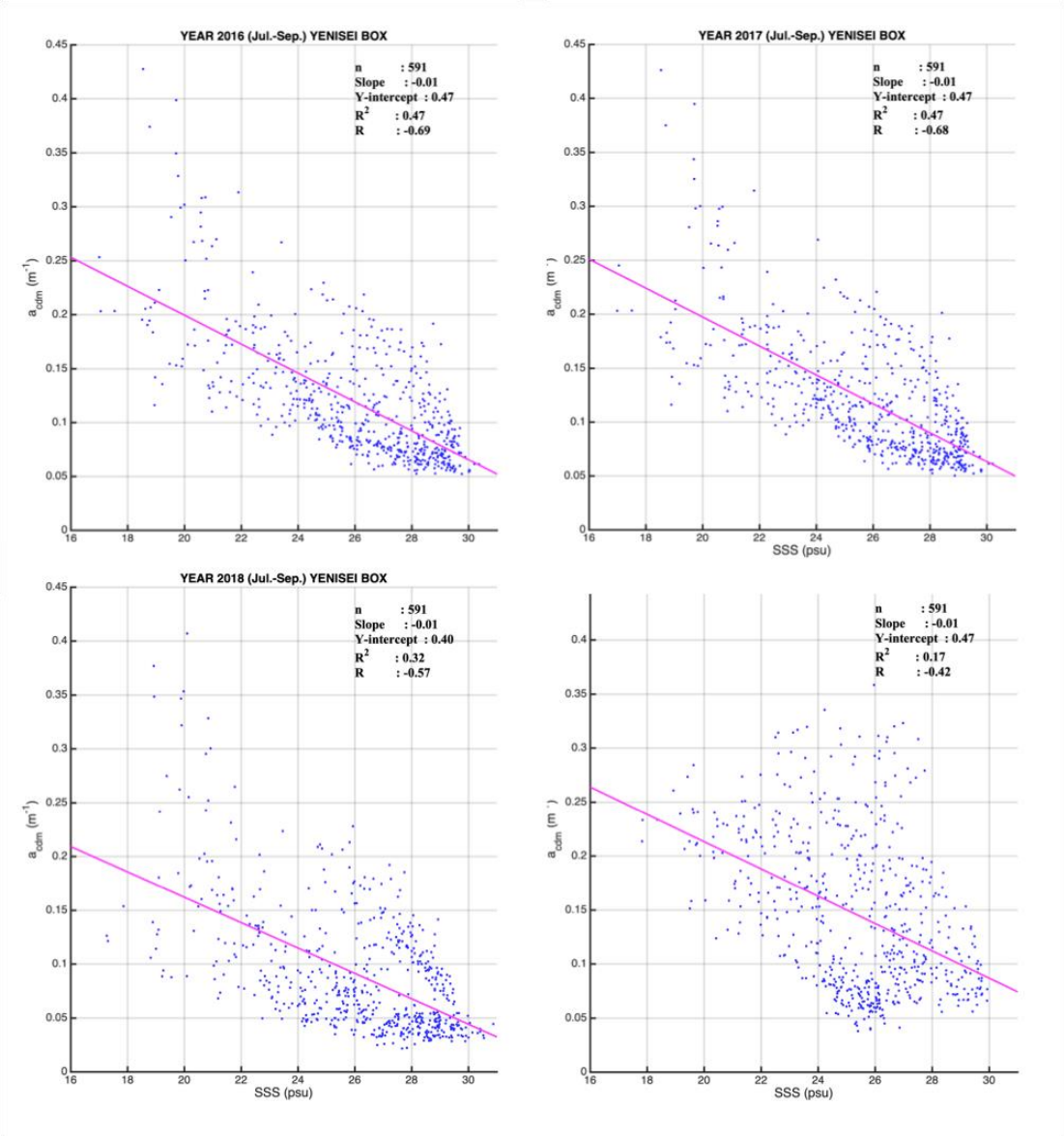

Figure 4.2-7 Interannual variability of mean CDM as a function of mean SMOS SSS over summer months (July to September) for years 2016 to 2019 inside the Yenisei-Ob rivers plume box. The magenta solid line represents the linear regression.

Inside the Yenisey-Ob rivers box, we also find a negative linear correlation between the mean SSS as a function of mean CDM, but with lower correlation coefficients, -0.69 and -0.68 for years 2016 and 2017 and descending to -0.57 and -0.42 for years 2018 and 2019. The correlations are lower in this river plume than in Lena.

The time series of mean SMOS SSS and CDM at Yenisei-Ob box (Figure 4.2-9) and Lena box (Figure 4.2-9) show a seasonal cycle in accordance with the River discharge cycles. The River discharge data set is downloaded from the Arctic Great Rivers Observatory webpage (http://www.arcticgreatrivers.org/) (Shiklomanov et. al, 2020). In this area, an intense inflow of freshwater starts in late spring-early summer and relaxes in autumn (Harms & Karcher, 2005). Once per year, as riverine waters reach a given area, SMOS SSS locally drops below 28 psu, and the CDM increases.

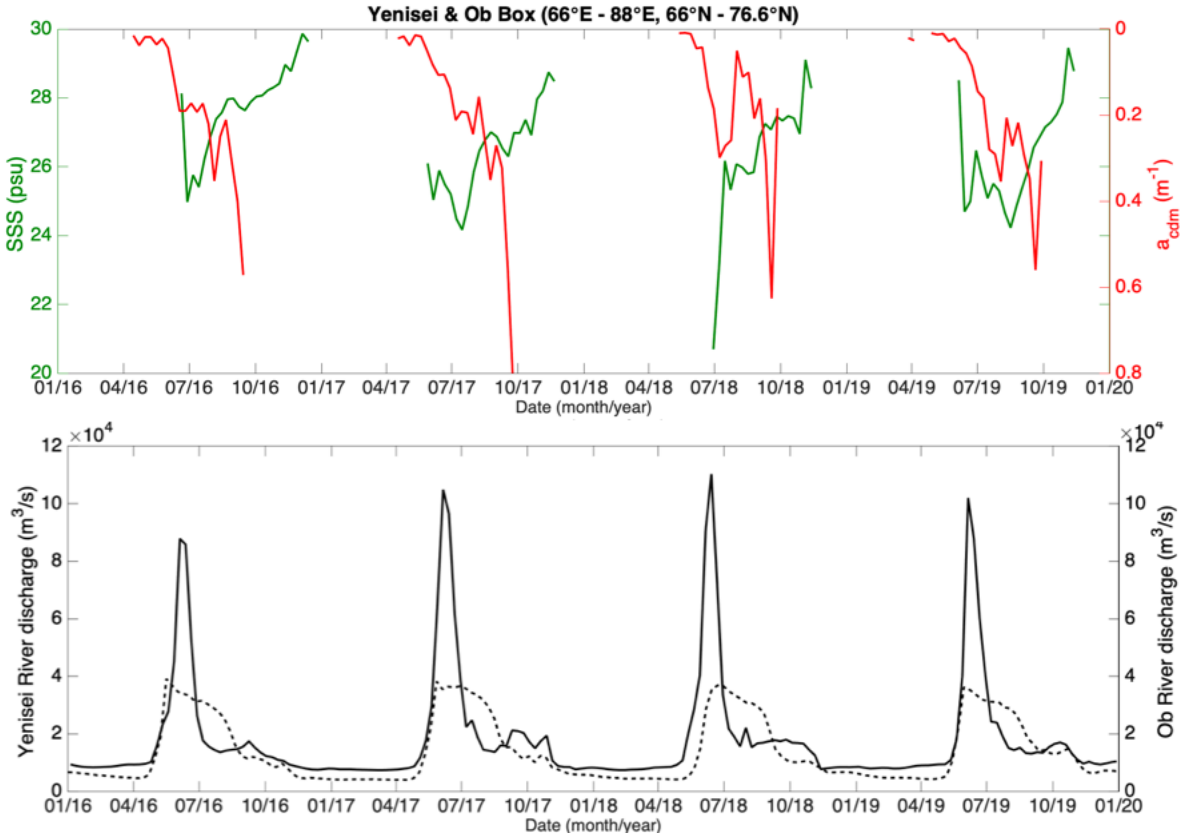

Figure 4.2-8 (a) Time series of the mean SMOS SSS (green) and the mean cdm (red) computed at Yenisei-Ob box (66-88^{o}E, 66-76.6^{o}N); (b) time series of the Yenisey (solid) discharge at Igarka gauge and Ob (dashed) discharge at Salekhard gauge.

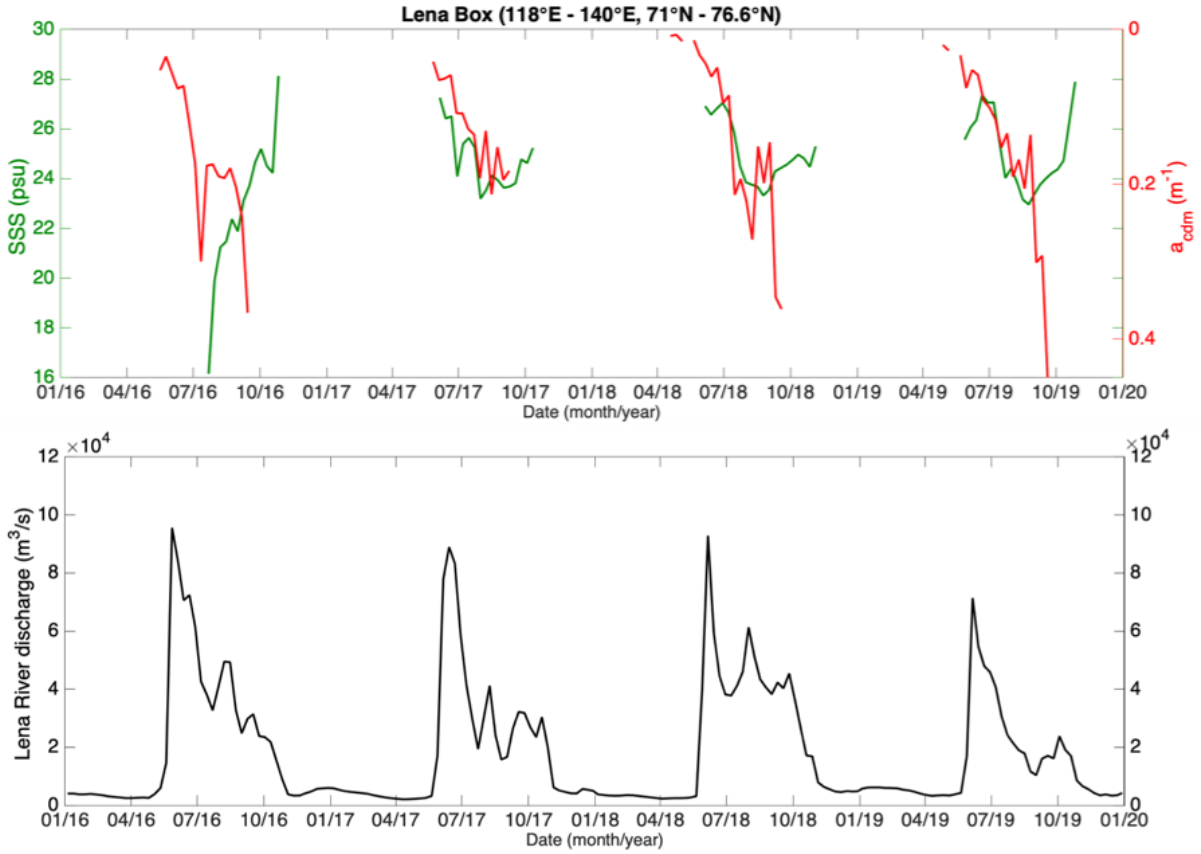

Figure 4.2-9 (a) Time series of the mean SMOS SSS (green) and the mean cdm (red) computed at Lena box (118-140°E, 71-76.6°N); (b) time series of the Lena discharge at Kyusyur gauge (Shiklomanov, et.al, 2020).

In the case of the Lena box we have the same pattern, i.e. when the river discharge increases in late spring, the surface salinity decreases and the CDM starts increasing (Figure 4.2-9), but in this case the Lena discharge is maintained longer and the salinity drop is maintained from late spring to autumn, as compared to Yenisei- Ob box.

To conclude, we find a stable negative linear correlation along the years 2016 to 2019 between SMOS SSS and CDM in the arctic river plumes and we find that regressions change depending on the area. Thanks to SMOS SSS Arctic + products we can better characterize the dynamics and interannual variability of the river plumes and assess the circulation of the region that is governed by differences in the buoyancy of fresher plume water and saltier ocean water, and changes of prevailing wind direction. Precipitation and evaporation play insignificant roles in the Kara Sea, as well as in the Arctic Ocean due to the large sea ice cover and low air temperatures (Lambert et al., 2019).

The expected future work is to extend the study period from 2012 to 2019, further study the interconnections between ice melting, CDM and SSS, and see if it is possible to infer one variable from the other similar to the work by Fournier et. al, 2015.

4.3 Study of Sea Surface Salinity trends with SMOS data

A study of the scientific impact assessment of the new product is to compute the SSS trends with the 9 years of the new Arctic+ Salinity SSS product.

We have dismissed 2011 data to perform the analysis, due to a strong RFI located in Trondheim which mainly affected the Norwegian and Greenland sea with less impact on Kara, Laptev, Beaufort. This RFI was turned off in 2012, so the 2012 measurements might also be affected in particular in the Norwegian, Greenland and Barents Seas. Therefore, the analysis in the mentioned regions is done excluding also 2012.

The Arctic and sub-Arctic Ocean have been divided into different regions (Figure 4.3-1): Norwegian Sea, Greenland Sea, Barents Sea, Beaufort Sea, Laptev Sea, and Kara Sea. The lat-lon limits of the regions are the shown in Table 3.2.4-1, but take into account that only the ice free regions for the whole period for each month are considered.

Table 3.2.4-1 Latitude and longitude of the selected regions. However, the final region is different per each month, since only the free sea ice pixels for the whole period are considered

Regions	latitude boxes	longitude boxes
Norwegian Sea	60 ºN to 80 ºN	East from the linear slope following the Mohn Ridge and the Knipovich Ridge
South Norwegian Sea	60 ºN to 68 ºN	-6 ºE to 10 ºE
Greenland Sea	67 ºN to 80 ºN	West part of Ridges
Barents Sea	70 ºN to 76.5 ºN	18 ºE to 55 ºE
Beaufort Sea	65 ºN to 80 ºN	165 ºW to 120 ºW
Kara Sea	65 ºN to 80 ºN	56 ºE to 100 ºE
Laptev Sea	65 ºN to 80 ºN	102 ºE to 140 ºE

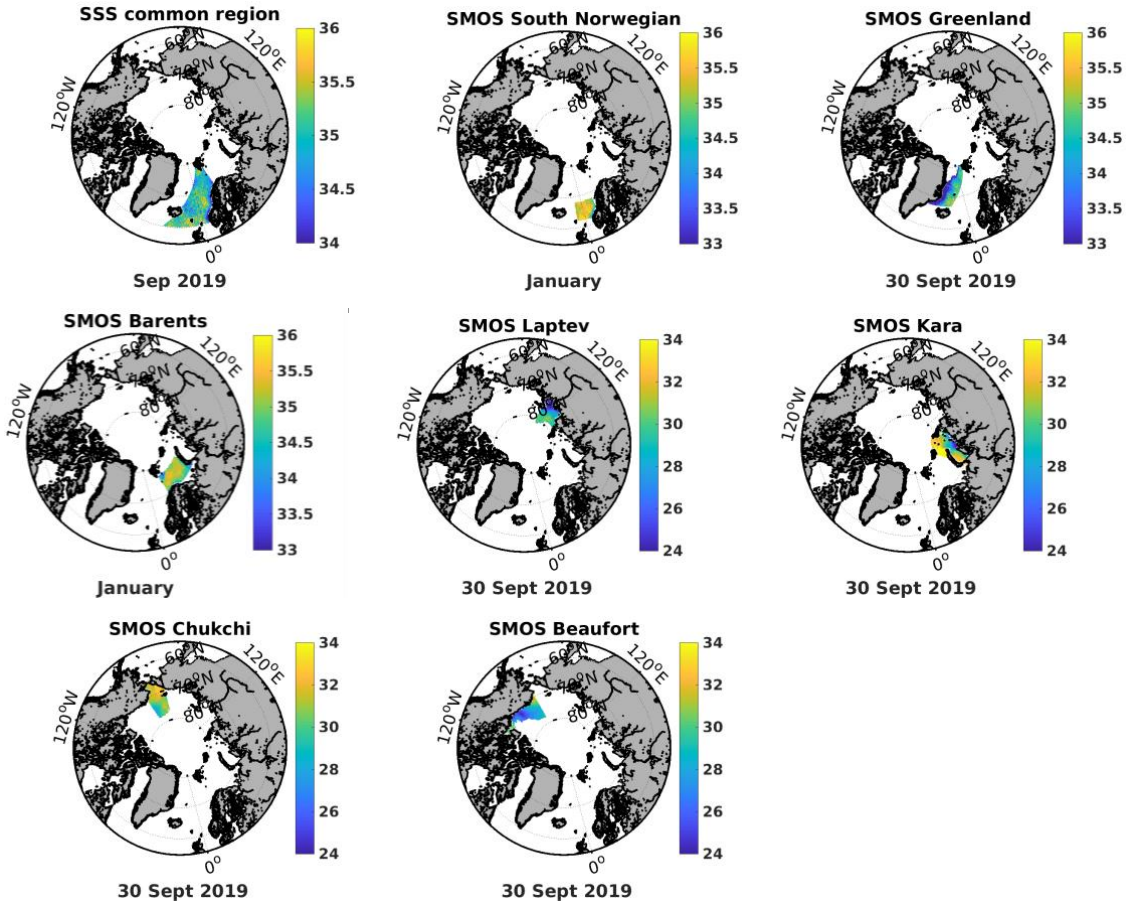

Figure 4.3-1 Sea surface salinity in September 2019 for the selected regions of the trends study.

The Greenland and Norwegian regions have been split following the Mohn Ridge and the Knipovich Ridge, to separate the natural ocean circulation as shown in Figure 4.3-2. Moreover, we have also analysed the southern Norwegian Sea region (from 60˚N to 68˚N), which should be more affected by the Atlantic waters. Very large annual salinity variability is observed in the global Arctic region (Arctic+Salinity product domain, above 60ºN) (see Figure 4.3-2b). The variability strongly depends on the region (Figure 4.3-2b). However, all the analysed regions show an intra-annual variability of more than 1 psu, showing that the Arctic has a large dynamic range of salinity values.

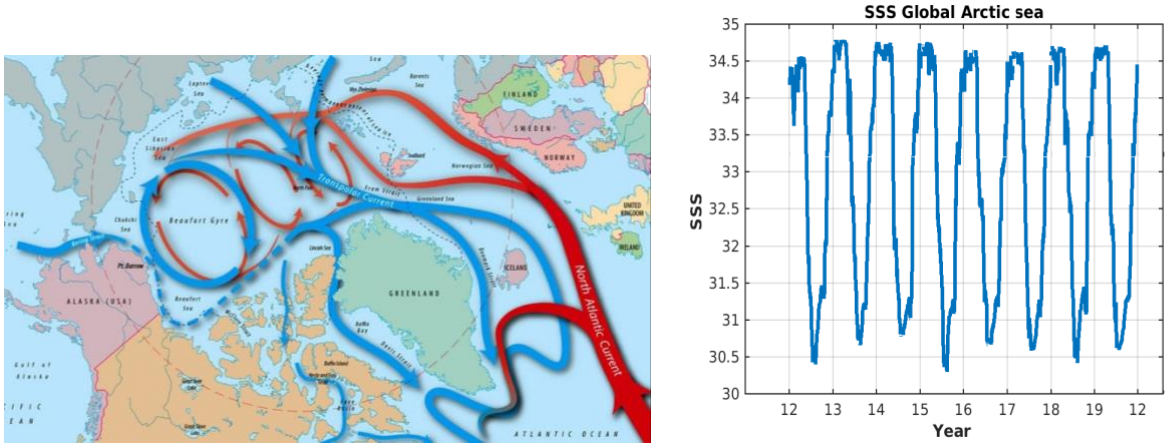

a) b)

Figure 4.3-2 :a) North Atlantic and Arctic ocean Circulation. b) global Arctic SMOS SSS variability from 2012 to 2019.

To compute the regional SSS trends we have used the following methodology:

- We compute the monthly mean SSS anomalies corrected for seasonality. The anomaly is computed by subtracting the monthly mean average from 2012/13-2019 to the monthly mean for each year, to avoid the intra-annual variability.
- Only pixels with a minimum of 28 days of valid measurements per month are considered on the computation of the mean value.
- A minimum of 2% of data of the selected region is considered to compute the mean regional SSS values.
- In some cases, only September data is used since this is the month with minimum sea ice extension.
- TOPAZ4 reanalysis data with the same region and time period is considered to compare the results. TOPAZ4 does not take into consideration the Greenland mass loss nor the interannual variability from Arctic rivers. TOPAZ4 uses a restoration to surface climatological SSS, at relatively a low rate (200 days on the top 3 m), except below sea ice and where the SSS differences from climatology are large, more than 0.5 psu.
- The region of analysis is selected considering only ice free and valid data pixels during the complete time period (2013-2019) per month. Therefore the monthly region is the same for all the years, avoiding the biases due to different sea ice extension during the 8 years. The selected areas are used for both SMOS and TOPAZ4 trends analysis.
- The trend is computed by deriving the linear regression line.

Figure 4.3-3 show the monthly SSS anomaly and the trend from 2013 -2019 with SMOS and TOPAZ models at different regions.

The Norwegian Sea shows a positive SMOS trend with the 7 years analysed. See that 2012 is not considered on the computation, since it is affected by an RFI event as explained above. When we focus on the southern Norwegian region (62º N to 68º N) the trend is more pronounced showing a slope of 0.2 psu/ decade. On the contrary, the TOPAZ4 SSS product shows a negative trend in the same period which is more consistent with the freshening observed by Mork et al. (2019) from in situ measurements between

2011 and 2018. It seems that the freshening observed in Mork et al. might be due to the freshening of the North Atlantic region (Holliday et al. 2020) that provides Atlantic waters into the Barents Sea.

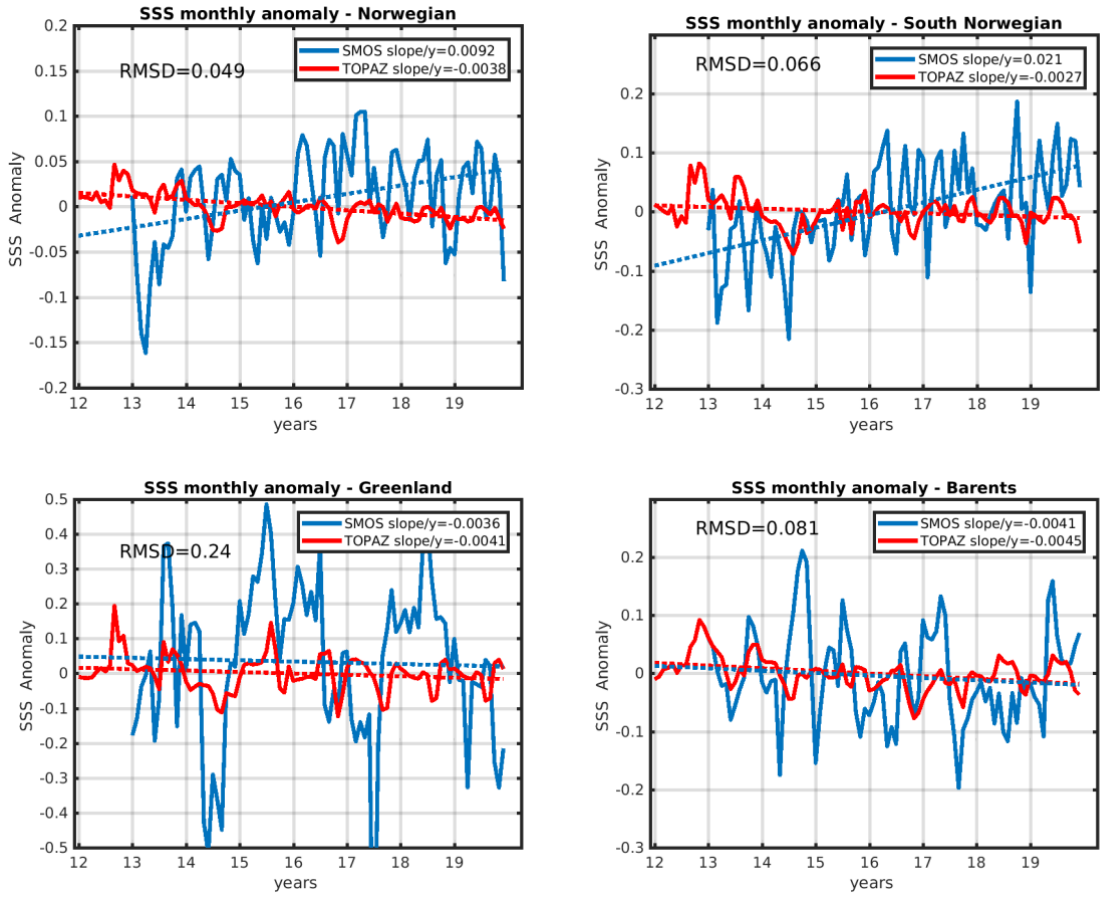

Figure 4.3-3 Monthly anomaly trends for SMOS and TOPAZ models for different Seas with the methodology (common region for the whole period under study). RMSD is the room mean square error of the regression line. Note: error bars of the mean points are not plotted because the std/sqrt(N) is very low, and is not visible on the plot.

Further north, in the Barents sea, the Atlantification is the name to describe the processes of the Atlantic water extending further poleward and/or occupying a larger part of the water column—both resulting in a warming of the region (Polyakov et al., 2017, Asbjørnsen el at. 2020) and increased salinities. Different mechanisms have, however, been proposed explaining such Atlantification. Changes in the strength and properties of the inflowing Atlantic water have been shown to affect winter sea ice growth and consequently the size of the ice-free in the Barents Sea (Årthun et al., 2012; Sandø et al., 2010). Changes in stratification (haloclines have weakened), leading to an increased vertical mixing and oceanic heat flux from the submerged Atlantic water layer, have been proposed as an important mechanism for upper-ocean warming in the north-western Barents Sea (Lind et al., 2018) and the Eurasian Basin of the Arctic Ocean (Polyakov et al., 2017). However, the increasing surface salinity trend revealed in Lind et al. (2018) (their Fig. 2e) have reached a plateau between 2010 and 2020 due to the vagaries of decadal climate variations. We, therefore, expect no significant trend in the Barents Sea in the SMOS period.

The Barents and Greenland regions analysis show a slightly negative trend, but the slope is weak (less than 0.5%). These values are thus coherent with TOPAZ4 trends and Lind et al. (2018).

Following the results from Section 3.4, the negative trend in the Greenland regions is unlikely to be caused by the meltwater from Greenland Ice Sheet although it is indisputably increasing in our present climate (Bamber et al., 2018). Recent variations in the export of freshwater (FW) from the Arctic Ocean by the Fram Strait will therefore need to be considered. De Steur et al. 2018 provided a recent update on the Fram Strait liquid freshwater export and variability and they found that the freshwater export has increased through Fram Strait. They state that the Eastern Greenland Current through Fram Strait conveyed a significant FW anomaly to the subpolar North Atlantic from 2009 to 2014. SMOS detects a large SSS decrease in 2014, which is repeated in 2017 and 2019. Similar analysis from de Steur et al 2018 should be done from 2016 (their data analysis finished by mid 2016). The observed increase of freshwater transport could well be responsible for the slight decrease trend of the SSS observed by SMOS.

The regions inside the Arctic Basin are more delicate because the sea ice cover does not permit to measure SSS from satellite, therefore we have computed the trend considering only September data, since this is the minimum sea ice extension. The September anomaly analysis is shown in Figure 4.2.4 for several regions from 2013 to 2019.

The September Barents Sea anomaly trend shows a more pronounced negative slope (m=-0.02 psu/y) than the annual monthly anomaly (m=-0.004 psu/y). This is expected since the analysis is done once the sea ice melting process is completed, so more ice-melted freshwater is present at the surface. Therefore, the September SSS salinity trend observed by SMOS has a rate of m=-0.21psu/decade. Topaz data show an almost flat trend, which may be affected by several setup parameters (too thin sea ice, relaxation to climatology, climatological rivers, climatological Pacific inflow).

The Beaufort Sea region anomaly shows also clear negative trends with a rate of m=-0.65 psu/decade. This is coherent with the observed freshwater content increase in the region reported in several papers (Gilles et al 2012, Haine et al., 2017, Proshutinsky et al 2019). TOPAZ does not exhibit any trend during the analysed period. This flatness can be due to several aforementioned causes, but as well the inhomogeneous coverage of salinity profiles, which cause jumps in the time series when assimilated.

The Laptev Sea also shows a negative trend, i.e. a freshening of the surface water, with a rate of m=-0.21 psu/decade, while TOPAZ exhibits a positive slope. In the Kara Sea, both SMOS and TOPAZ show similar positive trends, with the TOPAZ output data presenting a larger slope. We hypothesize that Kara Sea might still be affected by the Atlantic waters, while Laptev is too far from the detected region (Barents Sea).

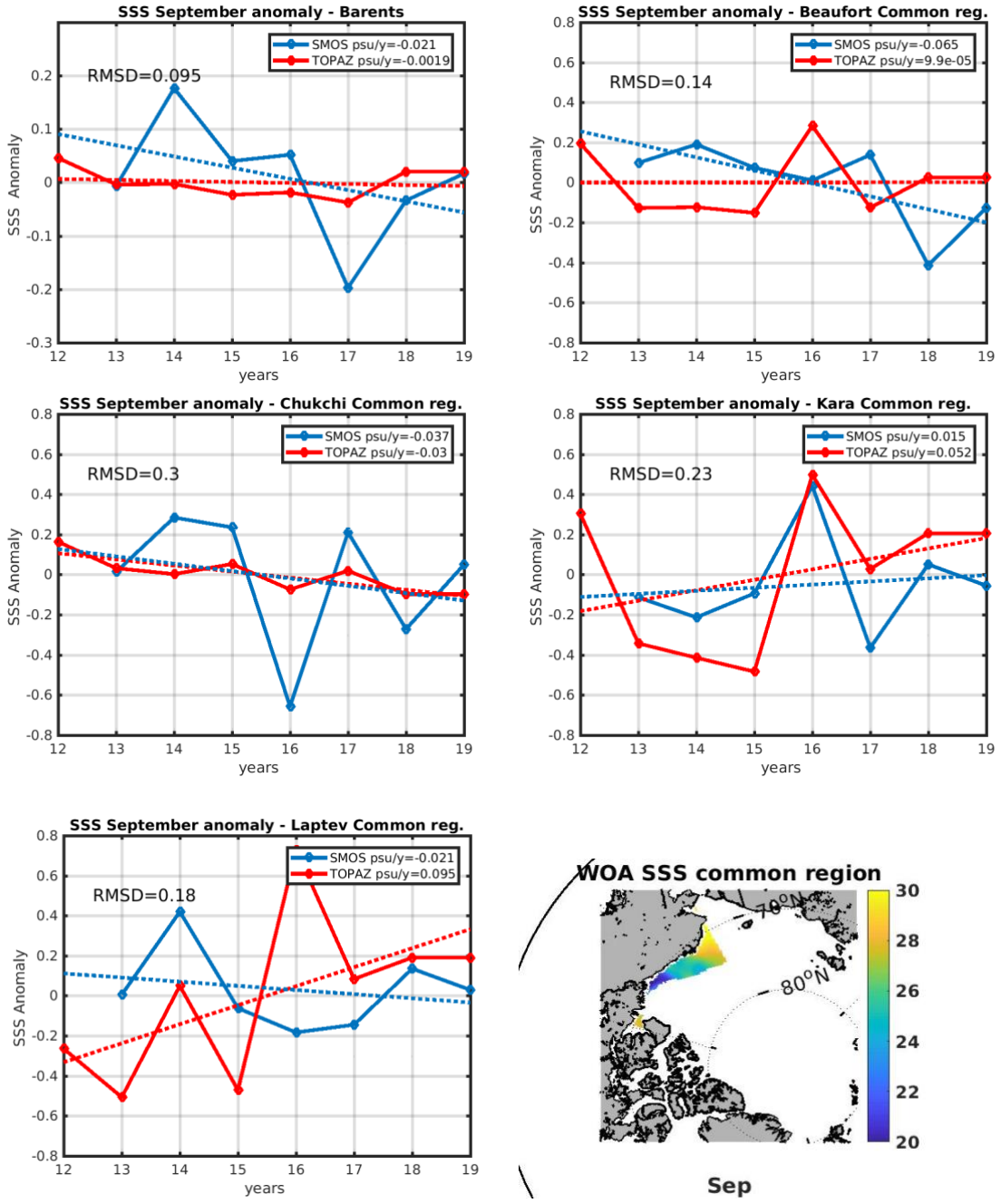

Figure 4.3-4 September anomaly trend for SMOS and TOPAZ model for different Arctic Seas. Last figure shows the Beaufort region considered in the September analysis.

The first assessment of SSS trends with SMOS shows promising results, but more work is required to better understand the results, characterize the error of the trends and compare the results with trends computed using in situ measurements reported in scientific papers.

5 Error analysis

Errors in satellite data products are known unknowns (Loew et al., 2017). Assessing the inherent uncertainties in satellite data products – and decomposing the inherent uncertainty components for each sub-component – is a challenging task.

To address the validation problem, we propose to use a technique used in different disciplines as the Triple Collocation.

Triple Collocation (TC) is a method originally introduced in [Stoffelen, 1998] to provide estimates of the measurement error variances of three systems measuring the same variable at the same time. TC is based on the statistical relations among the measurement variances and covariances in order to deduce the error variances for each measurement. Recently [González-Gambau, 2020], a variant of TC, especially adapted to deal with remote sensing measurements, has been introduced: the Correlated Triple Collocation (CTC). When applying CTC, the data are assumed to have the same space-time sampling. In contrast with standard TC, it is assumed that two of the datasets can have correlated errors (for instance, they are derived from the same basic measurement system). Besides, and taking into account that remote sensing series are typically not too long or maybe we are interested in assessing the evolution of the error of the systems as time passes, CTC is optimized to provide reasonably good estimates of the error variances even with a limited number of samples. With those conditions, CTC can be used to obtain maps of error variances of triples of remote sensing SSS maps, and obtain a different map for every year.

The results of the CTC analysis are largely explained in the Product Validation Report (PVR) of the same project, but we present here a short summary.

For the application of Correlated Triple Collocation, we have taken three sets of collocated SSS maps: JPL SMAP v4.2 SSS, 8-day maps; BEC SMOS Arctic SSSv 2.0, 9-day maps and BEC SMOS Arctic v3.1, 9-day maps. Different processing and Gaussian filters are applied to attain comparable represented scales.

With the products reduced to the common resolution (that of BEC v2.0), we have applied Correlated Triple Collocation (CTC), following [González-Gambau, 2020], in order to estimate the standard deviation of the errors of the three products. The results are shown in Figure 4.3-1.

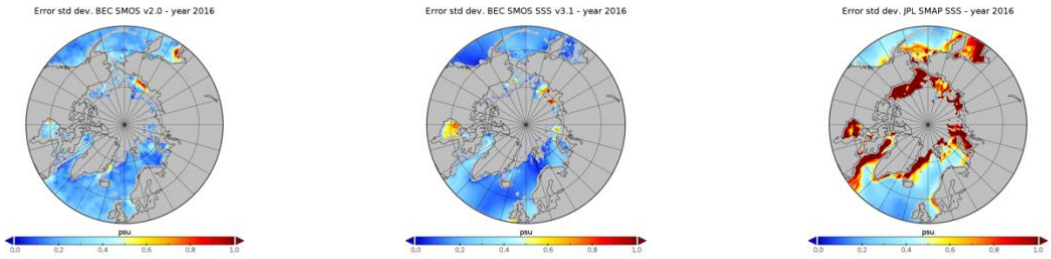

Figure 4.3-1 Error standard deviations computed via CTC for (from left to right) BEC SMOS Arctic SSS v2.0, BEC SMOS Arctic SSS v3.1 and JPL SMAP SSS v4.2, for all the collocated maps in the year 2016.

As shown in the figure, over the majority of the Arctic BEC v3.1 has the smallest error, excepting some specific regions where BEC v2.0 is better. JPL 4.2 is in all cases the product with the greatest error. The differences between the products are evidenced in Figure 4.3-2.

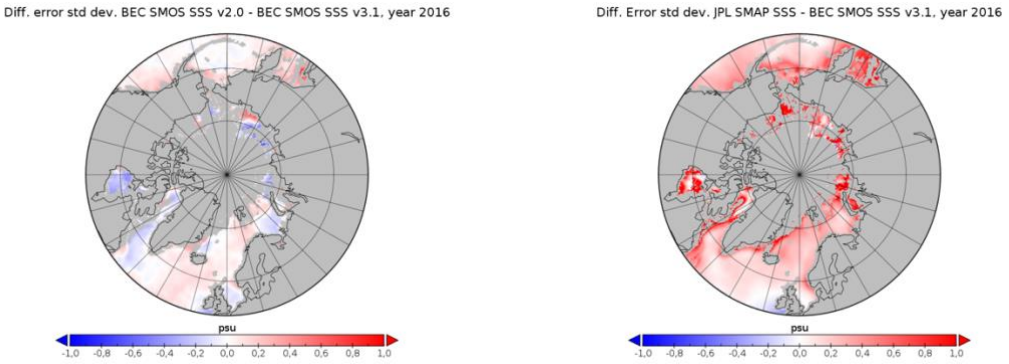

Figure 4.3-2 Difference between the error standard deviations of BEC SMOS SSS v2.0 (left) and of JPL SMAP SSS v4.2 (right) with BEC SMOS SSS v3.1 for the year 2016.

As shown in Figures, BEC v3.1 has smaller error than BEC v2.0 except in the Hudson Bay, Eastern coast of Greenland and Kara sea.

6 Summary and Conclusions

We conclude with reference to the objectives of the IAR that the SSS from SMOS can be assimilated in TOPAZ and its effect is generally beneficial considering a 6-months long test run. The effects in the selected regions are mostly positive, even in the coastal currents, or at worst neutral. The freshwater contents are changed by the assimilation of SSS, but in complex ways that do not relate directly to the SSS. In particular the freshwater contents of the Beaufort Sea changes seasonal cycle (both amplitude and phase), although there were no independent measurements of freshwater contents to compare against.

The work on the correlation between SMOS SSS and CDM we can conclude that we find a stable negative linear correlation along the years 2016 to 2019 between them in the Arctic river plumes and we find that regressions change depending on the area. Thanks to SMOS SSS Arctic+ products we can better characterize the dynamics and interannual variability of the river plumes and assess the circulation of the region that is governed by differences in the buoyancy of fresher plume water and saltier ocean water, and changes of prevailing wind direction. The expected future work is to extend the study period from 2012 to 2019, further study the interconnections between ice melting, CDM and SSS, and see if it is possible to infer one variable from the other similar to the work by Fournier et. al, 2015.

The salinity trend analysis shows promising results, even if the number of years analysed are reduced by the RFI. The results obtained are coherent with the scientific publications on many regions: the freshening observed in the Beaufort Sea, the flat trend in the Barents Sea in the past decade, the freshening observed in Laptev Sea. However, more work is required on this line as well as to promote collaboration with other teams who have in situ campaign measurements to verify the results.

An error analysis assessment has been performed inter-comparing JPL SMAP v4.2 SSS, BEC SMOS Arctic SSS v2.0, and BEC SMOS Arctic v3.1 products. The Correlated Triple Collocation method has been used and it shows that BEC v3.1 has smaller error than BEC v2.0 except in the Hudson Bay, Eastern coast of Greenland and Kara sea. JPL SMAP product is the one with larger errors of the analysed.

Further developments from this work are envisioned:

- Improvements of the TOPAZ reanalysis system aimed at better reproducing the interannual variability of freshwater fluxes: interannual river fluxes from the Arctic HYPE model, inclusion of Greenland Ice Sheet mass loss from the GriS CCI (se Section 3.4), interannual variability of the Pacific water fluxes through Fram Strain by downscaling from the global CMEMS reanalysis, improved sea ice thickness seasonal cycle and sea ice drift from a newer sea ice model.
- Work towards a better constrained freshwater budget in the Arctic, using SMOS SSS in combination with improved altimeter data, gravimetry data, sea ice thickness and drift data, river discharges and ocean water transports.
- Dedicated studies of the freshwater pulses originating from glacial melt episodes over Greenland and other Arctic glaciers on Novaya Zemlya, Svalbard…
- Preparatory work towards the CIMR high-priority Copernicus mission.

7 Bibliography

Asbjørnsen H., Årthun, M., Skagseth, Ø., & Eldevik, T. (2020). Mechanisms underlying recent Arctic Atlantification. Geophysical Research Letters, 47, e2020GL088036. https://doi.org/10.1029/2020GL088036

Årthun, M., Eldevik, T., Smedsrud, L. H., Skagseth, O., & Ingvaldsen, R. B. (2012). Quantifying the influence of Atlantic heat on Barents Sea ice variability and retreat. Journal of Climate, 25(13), 4736–4743. https://doi.org/10.1175/JCLI-D-11-00466.1

Bai, Y., Pan, D., Cai, W. J., He, X., Wang, D., Tao, B., & Zhu, Q. (2013). Remote sensing of salinity from satellite-derived CDOM in the Changjiang River dominated East China Sea. *Journal of Geophysical Research: Oceans*, *118*(1), 227-243.

Bamber, J. L., Tedstone, A. J., King, M. D., Howat, I. M., Enderlin, E. M., van den Broeke, M. R., & Noel, B. (2018). Land ice freshwater budget of the Arctic and North Atlantic Oceans: 1. Data, methods, and results. Journal of Geophysical Research: Oceans, 123, 1827–1837. https://doi.org/10.1002/2017JC013605

Del Castillo, C. E., & Miller, R. L. (2008). On the use of ocean color remote sensing to measure the transport of dissolved organic carbon by the Mississippi River Plume. *Remote Sensing of Environment*, *112*(3), 836-844.

de Steur, L., Peralta-Ferriz, C., & Pavlova, O. (2018). Freshwater export in the East Greenland Current freshens the North Atlantic. Geophysical Research Letters, 45, 13,359– 13,366. https://doi.org/10.1029/2018GL080207

Dubinina, E. O., Kossova, S. A., Miroshnikov, A. Y., & Fyaizullina, R. V. (2017a). Isotope parameters (δD, δ 18 O) and sources of freshwater input to Kara Sea. *Oceanology*, *57*(1), 31-40.

Dubinina, E. O., Kossova, S. A., Miroshnikov, A. Y., & Kokryatskaya, N. M. (2017b). Isotope (δD, δ 18 O) systematics in waters of the Russian Arctic seas. *Geochemistry International*, *55*(11), 1022-1032

Ferrari, G. M., & Dowell, M. D. (1998). CDOM absorption characteristics with relation to fluorescence and salinity in coastal areas of the southern Baltic Sea. *Estuarine, coastal and shelf science*, *47*(1), 91-105.

Fournier, S., Chapron, B., Salisbury, J., Vandemark, D., & Reul, N. (2015). Comparison of spaceborne measurements of sea surface salinity and colored detrital matter in the Amazon plume. *Journal of Geophysical Research: Oceans*, *120*(5), 3177-3192.

Giles, K. A., Laxon, S. W., Ridout, A. L., Wingham, D. J., & Bacon, S. (2012). Western Arctic Ocean freshwater storage increased by wind-driven spin-up of the Beaufort Gyre. Nature Geoscience, 5, 194–197. https://doi.org/10.1038/NGEO1379

Gonçalves-Araujo, R., Stedmon, C. A., Heim, B., Dubinenkov, I., Kraberg, A., Moiseev, D., & Bracher, A. (2015). From fresh to marine waters: Characterization and fate of dissolved organic matter in the Lena River Delta Region, Siberia. Frontiers in Marine Science, 2, 108.

González-Gambau, V., Turiel, A., González-Haro, C., Martínez, J., Olmedo, E., Oliva, R. & Martín-Neira, M. (2020). Triple collocation analysis for two error-correlated datasets: Application to L-band brightness temperatures over land. Remote Sensing 12, 3381, doi:10.3390/rs12203381.

Haine, T. W. N., Curry, B., Gerdes, R., Hansen, E., Karcher, M., Lee, C., et al. (2015). Arctic freshwater export: Status, mechanisms, and prospects. Global and Planetary Change, 125(2015), 13–35, ISSN 09218181. https://doi.org/10.1016/j.gloplacha.2014.11.013

Harms, I.H., & Karcher, M.J. (1999). Modelling the seasonal variability of circulation and hydrography in the Kara Sea. Journal of Geophysical Research, 104(C6), 13431–13438.

Harms, I.H., & Karcher, M.J. (2005). Kara Sea freshwater dispersion and export in the late 1990s. Journal of Geophysical Research: Oceans (1978–2012), 110(C8).

Heim, B., Juhls, B., Abramova, E., Bracher, A., Doerffer, R., Gonçalves-Araujo, R., ... & Overduin, P. (2019). Ocean colour remote sensing in the Laptev Sea. In *Remote Sensing of the Asian Seas* (pp. 123-138). Springer, Cham.

Holliday, N.P., Bersch, M., Berx, B. et al. Ocean circulation causes the largest freshening event for 120 years in eastern subpolar North Atlantic. Nat Commun 11, 585 (2020). https://doi.org/10.1038/s41467-020-14474-y

Hu, C., Muller-Karger, F. E., Biggs, D. C., Carder, K. L., Nababan, B., Nadeau, D., & Vanderbloemen, J. (2003). Comparison of ship and satellite bio-optical measurements on the continental margin of the NE Gulf of Mexico. *International Journal of Remote Sensing*, *24*(13), 2597-2612.

Korosov, A., Counillon, F., & Johannessen, J. A. (2015). Monitoring the spreading of the Amazon freshwater plume by MODIS, SMOS, Aquarius, and TOPAZ. Journal of Geophysical Research: Oceans, 120, 268–283. https://doi.org/doi:10.1002/ 2014JC010155

Kubryakov, A., Stanichny, S., & Zatsepin, A. (2016). River plume dynamics in the Kara Sea from altimetry-based lagrangian model, satellite salinity and chlorophyll data. *Remote sensing of environment*, *176*, 177-187.

Lambert, E., Nummelin, A., Pemberton, P., & Ilıcak, M. (2019). Tracing the imprint of river runoff variability on Arctic water mass transformation. *Journal of Geophysical Research: Oceans*, *124*(1), 302-319.

Lind, S., Ingvaldsen, R. B., & Furevik, T. (2018). Arctic warming hotspot in the northern Barents Sea linked to declining sea-ice import. Nature Climate Change, 8, 634–639. https://doi.org/10.1038/s41558-018-0205-y

Mork, K. A., Skagseth, O, Søiland, H. 'Recent Warming and Freshening of the Norwegian Sea Observed by Argo Data' J. Climate (2019) 32 (12): 3695–3705. https://doi.org/10.1175/JCLI-D-18-0591.1

Osadchiev, A. A., Frey, D. I., Shchuka, S. A., Tilinina, N. D., Morozov, E. G., & Zavialov, P. O. (2021). Structure of the freshened surface layer in the Kara Sea during ice-free periods. *Journal of Geophysical Research: Oceans*, e2020JC016486.

Polukhin, A. (2019). The role of river runoff in the Kara Sea surface layer acidification and carbonate system changes. *Environmental Research Letters*, *14*(10), 105007.

Polyakov, I. V., Pnyushkov, A. V., Alkire, M. B., Ashik, I. M., Baumann, T. M., Carmack, E. C., et al. (2017). Greater role for Atlantic inflows on sea-ice loss in the Eurasian Basin of the Arctic Ocean. Science, 356(6335), 285–291. https://doi.org/10.1126/science.aai8204

Proshutinsky, A., Krishfield, R., Toole, J. M., Timmermans, M.-L., Williams, W., Zimmermann, S., et al. (2019). Analysis of the Beaufort Gyre freshwater content in 2003–2018. Journal of Geophysical Research: Oceans, 124, 9658– 9689. https://doi.org/10.1029/2019JC015281

Shiklomanov, A.I., R.M. Holmes, J.W. McClelland, S.E. Tank, and R.G.M. Spencer. 2020. Arctic Great Rivers Observatory.

Spreen, G., de Steur, L., Divine, D., Gerland, S., Hansen, E., & Kwok, R. (2020). Arctic sea ice volume export through Fram Strait from 1992 to 2014. Journal of Geophysical Research: Oceans, 125, e2019JC016039. https://doi.org/10.1029/2019JC016039

Stoffelen, A. (1998). Toward the true near-surface wind speed: Error modeling and calibration using triple collocation. Journal of Geophysical Research 103, 7755–7766. DOI:10.1029/97JC03180.

Xie, J., Bertino, L., Counillon, F., Lisæter, K. A., and Sakov, P.: Quality assessment of the TOPAZ4 reanalysis in the Arctic over the period 1991–2013, Ocean Sci., 13, 123–144, https://doi.org/10.5194/os-13-123-2017, 2017.

Xie, J., Raj, R. P., Bertino, L., Samuelsen, A., and Wakamatsu, T.: Evaluation of Arctic Ocean surface salinities from the Soil Moisture and Ocean Salinity (SMOS) mission against a regional reanalysis and in situ data, Ocean Sci., 15, 1191–1206, https://doi.org/10.5194/os-15-1191-2019, 2019.

End of document